Renewable and Sustainable Energy Reviews 24 (2013) 418–444

Contents lists available at SciVerse ScienceDirect

Renewable and Sustainable Energy Reviews

journal homepage: www.elsevier.com/locate/rser

Thermal conductivity enhancement of nanostructure-based colloidal suspensions utilized as phase change materials for thermal energy storage: A review

J.M. Khodadadi *[,1], Liwu Fan [2], Hasan Babaei

Mechanical Engineering Department, Auburn University, 1418 Wiggins Hall, Auburn, AL 36849-5341, USA

A R T I C L E I N F O

Article history:
Received 7 March 2012
Received in revised form
10 March 2013
Accepted 15 March 2013
Available online 24 April 2013

Keywords:
Fusible materials
Melting
Nanofillers
Nanostructures
Phase change materials
Phase transformation
Solidification
Thermal conductivity enhancers

A B S T R A C T

A review of studies focused on enhancing the thermal conductivity of phase change materials (PCM) for thermal energy storage upon introduction of nanostructures is presented. These emerging materials have only been studied since 2005 and represent a clear departure from previous/existing practices of utilizing fixed, stationary high-conductivity inserts/structures into PCM. Carbon-based nanostructures (nanofibers, nanoplatelets and graphene flakes), carbon nanotubes, both metallic (Ag, Al, C/Cu and Cu) and metal oxide (Al_2O_3, CuO, MgO and TiO_2) nanoparticles and silver nanowires have been explored as the materials of the thermal conductivity promoters. Emphasis of the work so far has been placed on the dependence of the enhanced thermal conductivity on mass fraction of the nanostructures and temperature for both liquid and solid phases, however issues related to modifications of the degree of supercooling, melting temperature, viscosity, heat of fusion, etc. are also reported. In general, carbon-based nanostructures and carbon nanotubes exhibit far greater enhancement of thermal conductivity in comparison to metallic/metal oxide nanoparticles due to the high aspect-ratio of these nanofillers. Utilizing a figure of merit for the observed thermal conductivity enhancement, the majority of 340+ measured data points in both liquid and solid phases are summarized.

Contents

* Corresponding author. Tel.: +1 334 844 3333; fax: +1 334 844 3307.
E-mail address: khodajm@auburn.edu (J.M. Khodadadi).
[1] Alumni Professor.
[2] Institute of Thermal Science and Power Systems, Zhejiang University, Hangzhou 310027, PR China.

1364-0321/$ - see front matter © 2013 Elsevier Ltd. All rights reserved.
http://dx.doi.org/10.1016/j.rser.2013.03.031

1. Introduction

Wide-spread utilization of various renewable energy sources has received serious attention in recent years in light of unabated energy demands of the developing economies, unstable supply/pricing of fossil fuels and growing environmental concerns. Due to the unpredictable energy output of renewable energy-based systems, reliable, robust and efficient energy storage units need to be an integral component of these systems. Among all forms of energy, thermal energy is abundantly available as solar radiation, geothermal energy and thermally stratified layers in oceans. Moreover, thermal energy is also rejected by a great number of man-made energy conversion systems, industrial processes, propulsion/transportation systems, electronic devices, etc. Despite its ample quantity and ubiquity, thermal energy has been recognized as low-grade energy and widely branded as waste in industrial processes. Intercepting/recovery, storing and later utilization of thermal energy might be intended as an approach to increase thermal efficiency of a process or an industrial plant. Alternately, storage of thermal energy can be utilized for providing thermal comfort in dwellings/work spaces, energy conservation, improving operational life of electronics, etc. Consequently, these concerns and the wide range of applications of energy storage are closely linked to the storage capacity/size of any form of energy, including thermal energy.

2. Phase change materials for thermal energy storage

During heating/cooling of a bulk material, sensible and/or latent storage of thermal energy is achieved within that substance. The energy can then be available once the reverse process is applied. Owing to the stored/released latent heat (heat of fusion) during phase transition in the 100–1100 kJ/liter range, phase change materials (PCM) can be used to store thermal energy at a fixed temperature and within a smaller volume in comparison to the sensible storage option. Water, paraffins, fatty acids, sugar alcohols, salt hydrates, etc. are the most notable PCM among hundreds of materials for which the melting temperature varies over a wide range (−100 to 1000 °C) thus providing options for low- to high-temperature applications. Studies of PCM, their thermophysical properties, encapsulation, heat transfer enhancement and system-related issues have been conducted for decades. Improvement of properties and functionality of PCM is critical to their adoption since it is not an exaggeration to state that PCM in pure form are rarely utilized any longer. Among the shortcomings of pure PCM, their low thermal conductivity has been a major concern in view of the widely adopted and stringent requirement to store/release (charge/discharge) thermal energy over a desired time period. Consequently, enhancement of thermal conductivity of PCM has been the major focus of thermal energy storage research.

2.1. Routes for enhancing the thermal conductivity of PCM

Combining PCM of low thermal conductivity with highly conductive materials is a logical solution to come up with new materials possessing enhanced effective thermal conductivity. Placement of metallic fins, foams, wools into the PCM has been investigated and practiced for some time. Research articles addressing appropriate configurations of such *fixed, non-moving* structures in relation to conduction/convection and phase change thermal transport mechanisms have been published for decades. In a recent article, two of the authors [1] provided a review of the major findings in relation to the competing heat transfer mechanisms in thermal energy storage systems featuring meso-scale fixed, stationary thermal conductivity enhancers or inserts. Studies that concerned metallic foams and PCM/graphite composites were not covered thoroughly by Fan and Khodadadi [1].

Recognizing the variety of enabling enhancements/functionalities brought about due to greater utilization of nanotechnology, a far more challenging and also rewarding approach is to introduce nanostructures (nanoparticles, nanotubes, nanofibers, etc.) into PCM. The resulting nanostructure-enhanced PCM (NePCM) could provide extra functionalities and improvements not available to date, including thermal conductivity enhancement. In this connection, composites of solids and nanostructures to form structural materials have been widely investigated and dispersions of nanostructures in liquids (also termed nanofluids) have received wide-spread attention by the research community [2]. However, PCM are unique materials that are utilized in demanding freeze/thaw cycles. Thus, PCM are expected to perform in both liquid and solid phases and their modification using nanostructures has only been attempted over the past few years.

2.2. Attributes of an ideal NePCM

The colloidal suspensions that are formed by combining pure PCM and nanostructures are deemed to be *free-form* materials that will possess liquid-like properties once the PCM has melted. In this review great care is taken to minimize usage of the word "composites" that is meant to be related to *fixed-form* structures. In some cases this distinction is not easy to make and further communications with and implied comments by the original authors are pursued. An NePCM that possesses fluidity once the PCM component has melted can take the shape of the volume available to it with little contact heat transfer complications. In addition, it can accommodate convective currents that are widely accepted to be critical during the melting phase of the thaw/freeze cycles.

In view of the nano-scale focus of this review, studies that report on combining micron-size structures with PCM have been disregarded. Graphite/PCM composites are not covered since these are generally fixed-form structural composites and lack fluidity upon melting of PCM. No coverage of the thermal interface materials (TIM) is provided even though some similarities exist. It is reasoned that TIM serve to fill a non-ideal interface and do not generally serve a thermal storage function. Nanostructures and micron-scale additives have been utilized for suppression of supercooling and since they do not serve thermal storage purposes, such studies will not be reviewed.

Before reviewing the existing studies on NePCM, the reader is reminded that a body of literature exists in relation to theoretical prediction of the effective thermal conductivity of mixtures/composites. Many of the reviewed studies have also attempted to compare their measurements to some of these theoretical models. Thus, a very brief overview of these models follows.

3. Prediction of the effective thermal conductivity of NePCM colloids

Prediction of the effective transport properties, e.g., thermal conductivity, electrical conductivity, etc., of two-phase mixtures/composites has been of great interest for some time, e.g. Batchelor [3]. The essential assumption is that such a heterogeneous media (mixture/composite) consists of a continuous base material (matrix material) and a discrete phase (additives, e.g. nanostructures in the current context) dispersed in it [4]. For the NePCM colloids considered, the base PCM – either in solid or liquid states – is the continuous phase and the nano-structured thermal conductivity enhancers constitute as the discrete phase. The effective thermal conductivity of a two-phase mixture/composite depends on the thermal conductivity of both constituents, the concentration, dimension, geometry and distribution of the dispersed particles, and the interfacial effects between the matrix material and nanostructures as well. In view of the inherent randomness associated with the dispersed particles, microstructures of the mixtures/composites, i.e., dimension, geometry and distribution of the additives, have often been excluded in the theoretical work. Therefore, the effective thermal conductivity of two-phase mixtures/composites has mostly been correlated to the thermal conductivities of the matrix material and particles and concentration (volume fraction) of particles.

The simplest model for predicting the effective thermal conductivity (k) of two-phase mixtures/composites is the *mixture rule* that takes the following form [2]:

$$k_{eff}^{n} = (1-\phi)k_{c}^{n} + \phi k_{d}^{n}, \tag{1}$$

where subscripts *eff*, *c* and *d* stand for effective, continuous and discrete phases, respectively and ϕ is the volume fraction of the discrete phase. It is noted that the two extreme cases, i.e., parallel and series mixture rules, are obtained when the index n takes the values of 1 and −1, respectively. The predicted values corresponding to these two cases serve as the upper (parallel) and lower (series) bounds of the predicted effective thermal conductivity. The mixture rule, however, is only applicable for mixtures/composites with special distributions of particles, e.g., the particles are packed with a high concentration. For mixtures/composites with dilute concentrations (e.g., colloidal suspensions), the applicability of the mixture rule is usually not verified.

For dilute two-phase mixtures/composites with non-interacting spherical particles and in the absence of thermal interfacial resistance, the effective thermal conductivity can be predicted using the relation

$$k_{eff} = k_{c}\left[\frac{k_{d}+2k_{c}-2\phi(k_{c}-k_{d})}{k_{d}+2k_{c}+\phi(k_{c}-k_{d})}\right]. \tag{2}$$

This equation was first derived by Maxwell [5] for the analogous electrical conductivity problem of two-phase conductors. Even though it is based on assumption of very dilute additives, abundant experimental data of thermal conductivity of nanofluids have shown that Maxwell's equation is applicable for volume fraction of nanoparticles up to 10% [6].

As mentioned, the microstructures of particles and interfacial effects are not accounted for in Maxwell's equation. Some extensions based on Maxwell's equation have therefore been explored to address these concerns. For example, Nomura and Chou [7] presented a theoretical work on the bounds of the effective thermal conductivity of composites with short fibers as the discrete phase. Hasselman and Johnson [8] and Nan et al. [9] considered the interfacial thermal resistance in modeling effective thermal conductivity of particulate composites. Recently, Evans et al. [10] included the effects of aggregation of nanoparticles and interfacial thermal resistance on the effective thermal conductivity of nanocomposites and nanofluids. It should be noted that there are a great number of theoretical studies available in the literature and only a few representative ones were mentioned above.

Maxwell's equation and its extensions are usually classified as "static" models, indicating that the diffusion of particles, which may contribute to enhancement of heat exchange between the two phases, is not taken into consideration. This is well-justified if the continuous phase is stationary (e.g., NePCM in solid state). For colloidal suspensions or structural composites, the diffusion of particles, however, may play an important role, especially when the size of the particles is in sub-micron range (e.g., nanofluids). The Brownian motion, thermophoresis, and osmophoresis of such ultra-fine particles have been pointed out to be the possible mechanisms for thermal conductivity enhancement of nanofluids [11]. Although the contribution from diffusion of particles is still controversial, some "dynamic" models for predicting thermal conductivity of nanofluids have been proposed. For example, Koo and Kleinstreuer [12] postulated that the effective thermal conductivity of nanofluids consists of the static and dynamic parts, given by

$$k_{eff} = k_{static} + k_{dynamic}, \tag{3}$$

where k_{static} is estimated using Eq. (2) and the dynamic part $k_{dynamic}$ is related to the Brownian motion of nanoparticles. It is obvious that the diffusion of nanoparticles is considered to contribute positively to the enhanced thermal conductivity of nanofluids.

Based on abundant experimental data obtained by over 30 groups worldwide on identical samples, Buongiorno et al. [13] found that the measured thermal conductivity of nanofluids (volume fraction less than 3%) was in good agreement of Maxwell's equation and the extended model proposed by Nan et al. [9] and no anomalous enhancement beyond the static part was observed.

3.1. Conversion between the volume and mass fractions

Whereas the theoretical models for prediction of the effective thermal conductivity depend on the volume fraction of the components, the studies reviewed in this paper almost exclusively report values of mass fractions. For a two-component system, the conversions between the volume and mass (weight) fractions are

$$\phi_{wt} = \frac{\phi_{vol}\rho_{d}}{(1-\phi_{vol})\rho_{c}+\phi_{vol}\rho_{d}}, \tag{4}$$

and

$$\phi_{vol} = \frac{\phi_{wt}\rho_{c}}{\phi_{wt}\rho_{c}+(1-\phi_{wt})\rho_{d}}, \tag{5}$$

with ρ's standing for densities of the continuous and discrete phases, whereas the subscripts *vol* and *wt* denote volume and weight, respectively.

4. Studies on thermal conductivity enhancement

As discussed above, the reviewed literature will be limited to those embracing nanotechnology in PCM/thermal storage and such studies have only appeared since 2005. Thus, a chronological review of literature is warranted. At the same time, there are a few articles that appeared before 2005 in which thermal conductivity enhancement through introduction of high-conductivity particles was mentioned. These few contributions are also covered to allow the topic be kept in perspective.

4.1. Early studies directed at rejection of heat from space exploration systems

Fast-paced innovations in aeronautics and electronics in the middle of the twentieth century that were followed by the space

Table 1
Summary of utilized PCM and nano-structured thermal conductivity enhancers.

Authors (year)	PCM	Nano-structured materials		
	Materials and properties	Materials and properties	Dimensions, etc.	Fractions of enhancers
Siegel (1977) [15]	Molten salts, k: 0.4–4 W/mK	Stainless steel, iron (Fe), aluminum (Al), and copper (Cu) particles, k: 15, 60, 204, and 386 W/mK	N/A	0–100 vol%[a]
Seeniraj et al. (2002) [16]	Molten salts, k: 0.4–4 W/mK	Stainless steel, and Cu particles, k: 50, and 380 W/mK	N/A	0–100 vol%
Elgafy and Lafdi (2005) [17]	Paraffin wax, T_m: ~67 °C, k: ~0.24 W/mK, α: 1.61 × 10^{-7} m^2/s	Carbon nanofibers (CNF), ρ: ~1600 kg/m^3	Outer diameter:~100 nm, length: ~20 μm	1, 2, 3, and 4 wt%
Khodadadi and Hosseinizadeh (2007) [18]	Water, ρ: 997.1 kg/m^3, C_p: 4179 J/kg K, k: 0.6 W/mK, μ: 8.9 × 10^{-4} kg/ms, L: ~335,000 J/kg	Cu nanoparticles, ρ: 8954 kg/m^3, C_p: 383 J/kg K, k: 400 W/mK	10 nm	10 and 20 vol%
Hong et al. (2007) [19,20]	PAC[b], EG solutions (with 50 vol% water), T_f: −35.6 °C	Single-walled carbon nanotubes (SWCNT), alumina (Al_2O_3), MgO nanoparticles	N/A	0.05, 0.1, and 0.2 wt%
Zeng et al. (2007) [21]	1-Tetradecanol ($C_{14}H_{30}O$), T_m: ~38 °C, L: ~230,000 J/kg	Silver (Ag) nanoparticles	500 nm	2–94 wt%
Xie et al. (2008) [22]	Deionized (DI) water	Al_2O_3, titanium oxide (TiO_2) nanoparticles	~8 nm (Al_2O_3); ~3.8 nm (TiO_2)	1.54–6.19 wt% (Al_2O_3); 2.616–7.85 wt% (TiO_2)
Weinstein et al. (2008) [23]	Paraffin wax, T_m: 56 °C, C_p: 2100 J/kg K, k: 0.25 W/mK, L: ~234,000 J/kg	Graphite nanofibers (GNF) of three types: ribbon, platelet and herringbone	Diameter: 4–10 nm, length:~1 μm	0.25, 0.5, 1 and 5 wt%
Zeng et al. (2008) [24]	$C_{14}H_{30}O$ and $C_{14}H_{30}O$/PANI[c], T_m: ~35 °C, L: 221,250 J/kg and 119,140 J/kg	Multi-walled carbon nanotubes (MWCNT)	Outer diameter: 10–30 nm, length: 5–15 μm	0.5, 1, 2.5, and 5 wt%
Shaikh et al. (2008) [25]	Paraffin wax (shell wax 100), L: 156,300 J/kg	SWCNT, MWCNT, and CNF	Diameter: 1, 10, and 100 nm	0.1, 0.4, 0.7, and 1 vol%
Wang et al. (2008) [26]	Palmitic acid (PA), purity 98%, T_m: 62.5–64 °C, ρ: 853 kg/m^3, k: 0.24 W/mK, L: 207,800 J/kg	MWCNT, surface-oxidized by a mixed acid with 1:3 of concentrated nitric and sulfuric acids	Diameter: 30 nm, length: 50 μm, specific surface area: 60 m^2/g	0.5, 1, 2, and 5 wt%
Kim and Drzal (2009) [27]	n-Docosane, T_m: 53–57 °C, k: 0.26 W/mK, L: 157,300 J/kg	Exfoliated graphite nanoplatelets (xGnP)	Diameter: 15 μm, thickness: $<$ 10 nm, surface area: 30 m^2/g	1, 2, 3, 5, and 7 wt%
Zeng et al. (2009) [28]	PA, T_m: 59.48 °C, T_f: 58.78 °C, k: 0.318 W/mK, L: ~201,000 J/kg	Long and short pristine MWCNT; surface-oxidized MWCNT (by two acids)	Outer diameter: 10–30 nm, length: 5–15 μm (long), 1~2 μm (short)	0.099–4.76 wt% (without surfactants), and 0.095–4.5 wt% (with surfactants)
Liu et al. (2009) [29]	Saturated barium chloride ($BaCl_2$) aqueous solution, T_f: −8 °C, pH: 8	TiO_2 nanoparticles	20 nm	0.167, 0.283, 0.565, and 1.13 vol%
Wu et al. (2009) [30]	Distilled water, k: 0.6008 W/mK	Al_2O_3 nanoparticles	20 nm	0.05, 0.1, and 0.2 wt%
Ho and Gao (2009) [31] and Gao (2008) [32]	n-Octadecane ($C_{18}H_{38}$), T_m: 26.5 °C, T_f: 25.1 °C, L: ~243,100 J/kg	Al_2O_3 nanoparticles, ρ: 3600 kg/m^3	33 nm (159.6 and 196.0 nm in suspensions)	5 and 10 wt%
Wang et al. (2009) [35]	Paraffin wax, T_m: 53 °C, L: ~165,300 J/kg	MWCNT, treated by ball milling	Diameter: 30 nm, length: 50 μm, specific surface area: 60 m^2/g	0.2, 0.5, 1, and 2 wt%
Zeng et al. (2010) [36]	$C_{14}H_{30}O$, k: 0.32 W/mK, L: ~220,000 J/kg	Ag nanowires	N/A	9.09–62.73 wt%
Wang et al. (2010) [37]	PA, purity 98%, T_m: 62.4 °C, ρ: 853 kg/m^3, k: 0.22 W/mK (solid), 0.16 W/mK (liquid), L: 208,000 J/kg	MWCNT, treated by mechano-chemical reaction with potassium hydroxide/ball milling	Diameter: 30 nm, length: 50 μm, specific surface area: 60 m^2/g	0.2, 0.5, and 1 wt%
Wang et al. (2010) [38]	Paraffin wax, T_m: ~48.1 °C, L: 142,200 J/kg	γ-Al_2O_3 nanoparticles ρ: 3900 kg/m^3	20 nm	1, 2, and 5 wt%
Wang et al. (2010) [39]	PA, purity 98%, T_m: 62.5–64 °C, k: 0.223 W/mK (solid), 0.154 W/mK (liquid)	MWCNT, treated by surface oxidation, mechano-chemical reaction, ball milling, and grafting following acid oxidation	Diameter: 30 nm, length: 50 μm, specific surface area: 60 m^2/g	0.2, 0.5, and 1 wt%
Wang et al. (2010) [40]	Paraffin wax, purity 99.99%, T_m: 58–60 °C	Cu nanoparticles, purity: 99.9%	Diameter: 25 nm, specific surface area: 30–50 m^2/g	0.1, 0.5, 1, and 2 wt%
Wu et al. (2010) [41]			Diameter: 25 nm	

Table 1 (*continued*)

Authors (year)	PCM	Nano-structured materials		
	Materials and properties	Materials and properties	Dimensions, etc.	Fractions of enhancers
	Paraffin, T_m: 58–60 °C, k: 0.2699 W/mK (solid), 0.1687 W/mK (liquid), L: 204,000 J/kg	Cu, Al, and C/Cu nanoparticles, purity: 99.9%		0.1 wt% for all three kinds of nanoparticles, 0.1, 0.5, 1, and 2 wt% for Cu nanoparticles
Mo et al. (2011) [42]	DI water	MWCNT	Diameters: 10–30, 40–60, and 60–100 nm, length: 5–15 μm	0.1 wt%
Cui et al. (2011) [43]	Paraffin and soy wax, T_m: 52–54 °C	CNF, MWCNT (purity: 95%)	Outer diameter: 200 nm (CNF); diameter: 30 nm, length: 50 μm, specific surface area: 60 m^2/g (MWCNT)	1, 2, 5, and 10 wt%
Xiang and Drzal (2011) [44]	*n*-Docosane, T_m: 53–57 °C	Exfoliated graphite nanoplatelets (xGnP); xGnP with ball milling treatment	Diameter: 15 μm, thickness: $<$ 10 nm, surface area: 20–40 m^2/g, and diameter: 1 μm, surface area: 100–130 m^2/g after ball milling	1, 2, 4, 6, 8, and 10 wt%
Yavari et al. (2011) [47]	1-Octadecanol, T_m: ~66 °C, ρ: 812 kg/m^3, k: 0.38 W/mK, L: ~250,000 J/kg	Graphene flakes	N/A	0.2, 0.5, 1, 2, and 4 wt%
Fan and Khodadadi (2011) [48]	Cyclohexane, T_m: 6.5 °C, ρ: 850 kg/m^3 (solid), 779 kg/m^3 (liquid), L: 32,557 J/kg	Copper oxide (CuO) nanoparticles	Diameter: 5–15 nm	1, 2, and 4 wt%
Fan and Khodadadi (2011) [51]	Eicosane, T_m: ~37 °C	Copper oxide (CuO) nanoparticles	Diameter: 5–15 nm	1, 2, 5, and 10 wt%

[a] Vol% and wt% stand for volumetric and mass fractions, respectively.
[b] PAC and EG stand for prediluted antifreeze coolant and ethylene glycol, respectively.
[c] PANI denotes polyaniline.

exploration, called for the development of compact and robust thermal control and energy storage systems using PCM. Many of the relevant studies were discussed by Fan and Khodadadi [1]. Among those reviewed, Hoover et al. [14] reported results of experimental studies pertinent to spacecraft thermal control with a number of pure PCM and PCM/composites using metals and other materials. Important issues such as PCM system performance characteristics, determination of PCM and PCM/filler thermal diffusivities, the effects of long-term thermal cycling, PCM-container compatibility, catalyst effectiveness and stability, etc. were addressed. Three PCM, namely lithium nitrate trihydrate ($LiNO_3$–$3H_2O$) with zinc hydroxy nitrate catalyst, acetamide and myristic acid, were found acceptable for use in prototype aluminum thermal control devices. Using $LiNO_3$–$3H_2O$ as the PCM, *aluminum powder*, aluminum gauze, aluminum honeycomb, alumina (Al_2O_3) foam and *alumina powder* were used as fillers with 8/1 PCM/filler ratio (not clear as to being volume or mass-based). However, no details on size of the powders were given. From a historical point of view, Ref. [14] can be identified as the first attempt to explore the effect of adding a metallic and oxide powder (particles) for increasing thermal conductivity of PCM.

Following Hoover et al. [14], the number of studies devoted to thermal conductivity enhancement through introduction of particles with high conductivity becomes sparse. Starting in 2005, great effort has focused on exploring the role of nanostructures in enhancing thermal conductivity of phase change materials, the exposition of which will be presented in a chronological order. The relevant details of the reviewed papers are summarized in two elaborate Tables 1 and 2. The specific materials and their properties (both PCM and nanostructures) along with the size information and mass/volume fractions of the thermal conductivity enhancers are given in Table 1. Preparation techniques for the colloidal suspensions that are generally achieved by mixing followed by possible use of sonication and utilization of surfactants or lack of it for realizing stable dispersions are summarized in Table 2. As for the characterization techniques, specific attention is given to the employed method(s) for measuring thermal conductivity and the extent of its measurement (one or multiple temperatures and for which phases). Moreover, any stability concerns expressed by the authors and some details of any phase change heat transfer tests are summarized in Table 2. As of late 2011, the number of reviewed papers along with their publication year is summarized in Fig. 1. It is clear that since 2007, a steady rise of research activity on thermal conductivity enhancement of PCM through utilizing nanostructure enhancers is evident. Overall, 28 papers that directly concern thermal conductivity enhancement of PCM through introduction of nanostructures have appeared since 2005. All the figures (except Fig. 1 and those summarizing the work of the authors) and artwork in this paper are taken from the reviewed papers. Thus, the authors do not take responsibility for their quality and presentation.

4.2. Theoretical studies proposing “particle-enhanced” PCM

Following the work of Hoover et al. [14] in 1971 and prior to exploring nanotechnology for enhancing thermal conductivity, only two papers considered the general idea of thermal conductivity enhancement through dispersion of particles. Even though these two papers did not deal with nanoscales, they will be reviewed in order to maintain continuity of the topic.

In order to improve the heat extraction rate of thermal energy storage systems at elevated temperatures through enhancing the thermal conductivity of the solidified phase, Siegel [15] set forth a proposal to “disperse fine particles of a high-conductivity material” in molten salts. Even though settling of particles and their engulfment/rejection at the moving solidifying fronts was briefly

Table 2
Summary of preparation and characterization methods and instruments for studies of colloidal suspensions utilized as nano-enhanced phase change materials (NePCM).

Authors (year)	Preparation		Characterization			Study of heat transfer
	Methods	Dispersion and stabilization[a]	Thermal conductivity[b]	Other measurements and instruments	Stability concerns	
Siegel (1977) [15]	N/A	N/A	Maxwell's equation	N/A	N/A	Analytical solutions
Seeniraj et al. (2002) [16]	N/A	N/A	N/A	N/A	N/A	Theoretical analysis
Elgafy and Lafdi (2005) [17]	Two-step	N/A	Calculated using measured α and C_p	DSC[c], laser flash technique	N/A	TC[d] readings for a thaw/freeze test; analytical model for predicting thermal conductivity
Khodadadi and Hosseinizadeh (2007) [18]	N/A	N/A	Maxwell's equation	N/A	N/A	CFD modeling
Hong et al. (2007) [19,20]	Two-step	Sonication *surfactant*: SDBS[e]	N/A	pH, freezing point (ASTM D1177), microscope	Visually observed in transparent beakers	N/A
Zeng et al. (2007) [21]	One-step	N/A	N/A	DSC, FTIR[f], TEM, TGA, XRD	Two heating cycles	TC readings
Xie et al. (2008) [22]	Two-step	Sonication, magnetic force agitation	N/A	DSC, TEM, TGA, XRD	Severe aggregation of titanium oxide nanoparticles	N/A
Weinstein et al. (2008) [23]	Two-step	Sonication	Steady-state guided hot plate method, S-1T	DSC, TEM	Significant precipitation of GNF observed upon several melting/freezing cycles	TC readings for melting experiments in a cubic cavity
Zeng et al. (2008) [24]	Two-step	Sonication	Hot Disk Thermal Constants Analyzer (TPS[g]), S-1T	DSC, SEM[h], TGA	N/A	N/A
Shaikh et al. (2008) [25]	Two-step	Ultrasonication	N/A	DSC	N/A	Theoretical model by intermolecular attraction, and numerical simulation
Wang et al. (2008) [26]	Two-step	Sonication	THW[i], SL-mT	DSC, SEM	Observed by SEM images after thawing/freezing 80 times	N/A
Kim and Drzal (2009) [27]	Two-step	Ultrasonication	Steady-state guarded heat flow meter method, S-1T	DSC, Femtostat/Potentiostat, SEM, TGA	N/A	N/A
Zeng et al. (2009) [28]	Two-step	Sonication *surfactants*: CTAB[j], SDBS	Hot Disk Thermal Constants Analyzer (TPS), S-1T	DSC, FTIR	N/A	N/A
Liu et al. (2009) [29]	Two-step	Supersonic oscillator	THW, L-mT	TEM	N/A	Freeze/thaw cycling tests using a cold storage/supply system
Wu et al. (2009) [30]	Two-step	Ultrasonication *surfactant*: SDBS	THW, L-1T	Light scattering, zeta potential	Observed through particle size distribution and zeta potential	TC readings and infrared imaging for freeze/thaw tests
Ho and Gao (2009) [31] and Gao (2008) [32]	Two-step	Ultrasonication (with unspecified surfactant SINO-POL20)	THW, L-mT	DSC, hydrometer, laser diffraction, viscometer	N/A	Melting experiments in a rectangular cavity
Wang et al. (2009) [35]	Two-step	Sonication	THW, SL-mT	DSC, SEM	Being subjected to 70 °C for 96 h	N/A
Zeng et al. (2010) [36]	Two-step	Sonication (with anhydrous ethanol)	Hot Disk Thermal Constants Analyzer (TPS), S-1T	DSC, FTIR, SEM, TGA, XRD	N/A	N/A
Wang et al. (2010) [37]	Two-step	Sonication	THW, SL-mT	DSC, FTIR, SEM	N/A	N/A
Wang et al. (2010) [38]	Two-step	Sonication (with oleylamine)	THW, SL-mT	DSC, FTIR, SEM, TEM, XRD	N/A	N/A
Wang et al. (2010) [39]	Two-step	Sonication	THW, SL-mT	FTIR, SEM, TEM, XRD	N/A	N/A
Wang et al. (2010) [40]	Two-step	Ultrasonication *surfactant*: gum arabic	N/A	DSC, TEM	Visually observed	TC readings for a thaw/freeze test
Wu et al. (2010) [41]	Two-step	Ultrasonication *surfactants*: gum arabic, Span-80, CTAB, SDBS, and Hitenol BC-10	THW, SL (no temperature information)	DSC, FTIR	Visually observed, thermal stability test for up to 100 cycles by DSC	TC readings for a thaw/freeze test
Mo et al. (2011) [42]	Two-step	Ultrasonication *surfactant*: SDS[k]	N/A	SEM	N/A	TC readings for freeze tests

Table 2 (*continued*)

Authors (year)	Preparation		Characterization			Study of heat transfer
	Methods	Dispersion and stabilization[a]	Thermal conductivity[b]	Other measurements and instruments	Stability concerns	
Cui et al. (2011) [43]	Two-step	Ultrasonication	THW, S-1T	DSC, SEM	N/A	TC readings for heating tests of solids only
Xiang and Drzal (2011) [44]	Two-step	Ultrasonication	Steady-state guarded heat flow meter method, S-1T	DSC, Femtostat/ Potentiostat, SEM, TGA	N/A	N/A
Yavari et al. (2011) [47]	Two-step	Sonication	Steady-state method, S-1T	DSC, SEM, TEM	N/A	N/A
Fan and Khodadadi (2011) [48]	Two-step	*Surfactant*: SOA[l]	Hot Disk Thermal Constants Analyzer (TPS), SL-mT	N/A	N/A	TC readings for freezing tests
Fan and Khodadadi (2011) [51]	Two-step	*Surfactant*: SOA	Hot Disk Thermal Constants Analyzer (TPS), SL-mT	N/A	N/A	N/A

[a] This column is only applicable to the two-step method.
[b] Under thermal conductivity column, SL-xT stands for S=solid phase, L=liquid phase, x=1 for single and m for multiple, T=temperature measurements.
[c] DSC stands for differential scanning calorimetry.
[d] TC denotes thermocouples.
[e] SDBS denotes sodium dodecylbenzene sulfonate.
[f] FTIR, TEM, TGA, and XRD stand for Fourier transform infrared spectroscopy, transmission electron microscopy, thermal gravimetric analysis, and X-ray diffraction, respectively.
[g] TPS denotes transient plane source technique.
[h] SEM denotes scanning electron microscope.
[i] THW stands for transient hot wire method.
[j] CTAB denotes cetyltrimethyl ammonium bromide.
[k] SDS denotes sodium dodecyl sulfate.
[l] SOA denotes sodium oleate acid.

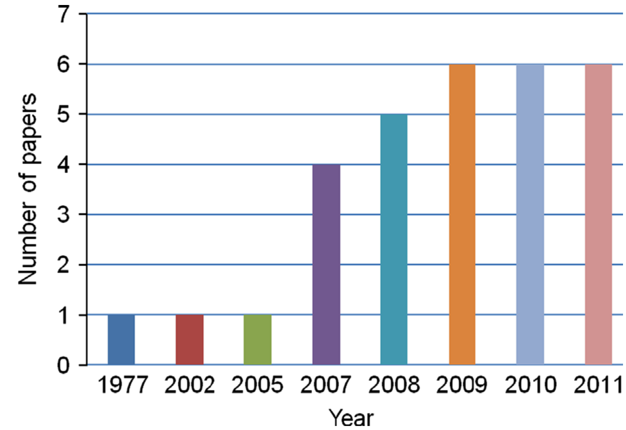


Fig. 1. Statistics of the published papers on NePCM until July 2011.

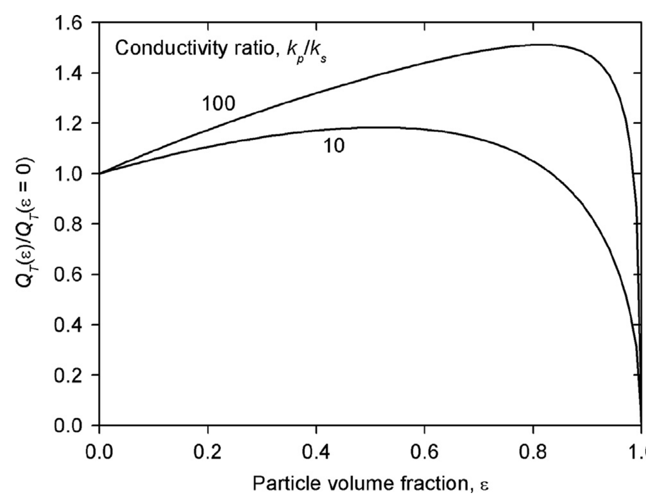


Fig. 2. Ratio of heat removal from a frozen slab with dispersed particles to that free of particles for two different thermal conductivity ratios [15].

mentioned, an idealized assumption was invoked stating that during melting and freezing cycles, the particles will remain uniformly suspended within the PCM. The diminished heat of fusion per unit volume of the PCM/particle system and the longer conduction path required for a given quantity of heat removal were identified as drawbacks compared to the advantage of a faster solidification rate due to the enhanced thermal conductivity of the medium. Through neglect of the subcooling energy of the frozen layer relative to heat of fusion, the analysis was markedly simplified. Assuming negligible wall resistance and ignoring heat convection to the heat transfer fluid, thermal resistance analyses linked to the extracted energy from the growing solidification layers on a flat plate, inside a tube and outside a tube were utilized. Combinations of high thermal conductivity particles (steel, iron, aluminum and copper) with target PCM (salts) were studied. With the particle to solid phase thermal conductivity ratio ranging between 10 and 100, the maximum values of the heat removal rate with particles compared to a particle-free PCM for a plane layer geometry were observed for particle volume fractions of about 0.5 and 0.8, respectively (Fig. 2). These corresponded to increased energy extraction rates of about 20 and 50%. Impracticality of such high particle volume fractions in addition to the possible breakdown of the utilized expression for thermal conductivity of mixtures due to Maxwell [5] was noted. In addition, a geometry effect was also observed with the presence of particles being less pronounced on the inside of a tube compared to the outside.

Seeniraj et al. [16] investigated the influence of dispersed fine particles with high thermal conductivity in a PCM on the movement of the melting front in a latent heat thermal storage shell and tube heat exchanger unit. Melting of the particle-laden PCM was driven by the flow of a heat transfer fluid within an inner tube under laminar and turbulent fully developed conditions. Neglecting thermal resistance of the tube wall and assuming thermal equilibrium of the particles with the PCM, a quasi-steady formulation was developed. The investigated ranges of the thermal conductivity ratio and volume fraction were similar to Siegel [15]. Increase of the volume fraction of particles reduced the cumulative energy storage capacity over a time interval and decreased the instantaneous surface heat flux. This, in turn, led to existence of an optimum volume fraction of the dispersed particles for maximum energy storage/extraction.

Based on the above discussions, the past efforts on thermal conductivity enhancement of PCM through introducing particle additives have been identified. We now focus on the core review in the paper that deals with nanostructure-based colloidal suspensions as novel thermal energy storage materials.

4.3. Studies of nanostructures-based colloidal suspensions utilized as novel PCM

Mixtures of pure paraffin with a melting temperature (MT) of 67 °C and carbon nanofibers (CNF) obtained from Applied Sciences, Cedarville, OH, having density, average diameter and length of 1600 kg/m^3, 100 nm and 20 μm, respectively, were prepared using shear mixing and melting techniques by Elgafy and Lafdi [17]. Thermal diffusivity of the solid composites (wt% equal to 1, 2, 3 and 4) was measured at room temperature using the laser flash technique (disk of 18 mm diameter and 3.3 mm thickness), whereas differential scanning calorimetry (DSC) was used for measuring the heat capacity. Thermal conductivity was then calculated by combining measured values of the thermal diffusivity, density and heat capacity. The thermal diffusivity and conductivity data at room temperature along with heat capacity values vs. temperature are shown in Fig. 3a–c. The linear dependence of the thermal diffusivity and conductivity data on the loading of carbon nanofibers is observed, whereas the heat capacity is markedly lowered upon raising the volume fraction (e.g. 35% at the highest reported temperature). Each sample that had a mass of 20 g (wt% being equal to 1, 2, 3 and 4) was placed in a cylindrical glass enclosure (2 cm in diameter and 2.5 cm in height) with insulated top and bottom, thus accommodating radial transfer of heat. The samples were then placed simultaneously inside a furnace core that maintained a uniform heat flux. After a sufficient period of time for melting of the samples (about 4 h), transient temperature of each sample during cool down was

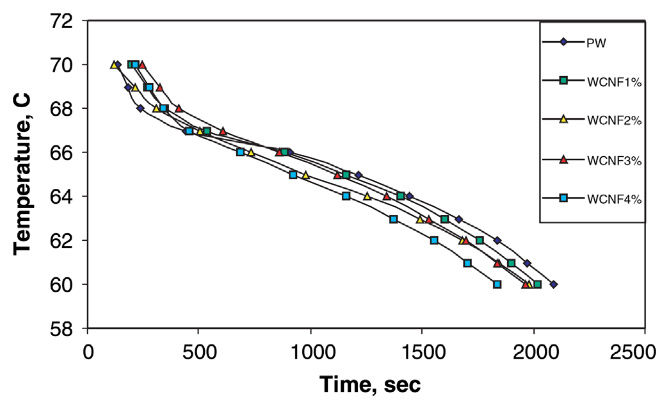


Fig. 4. Transient temperature variations during a solidification process for samples with different mass fractions of carbon nanofibers [17].

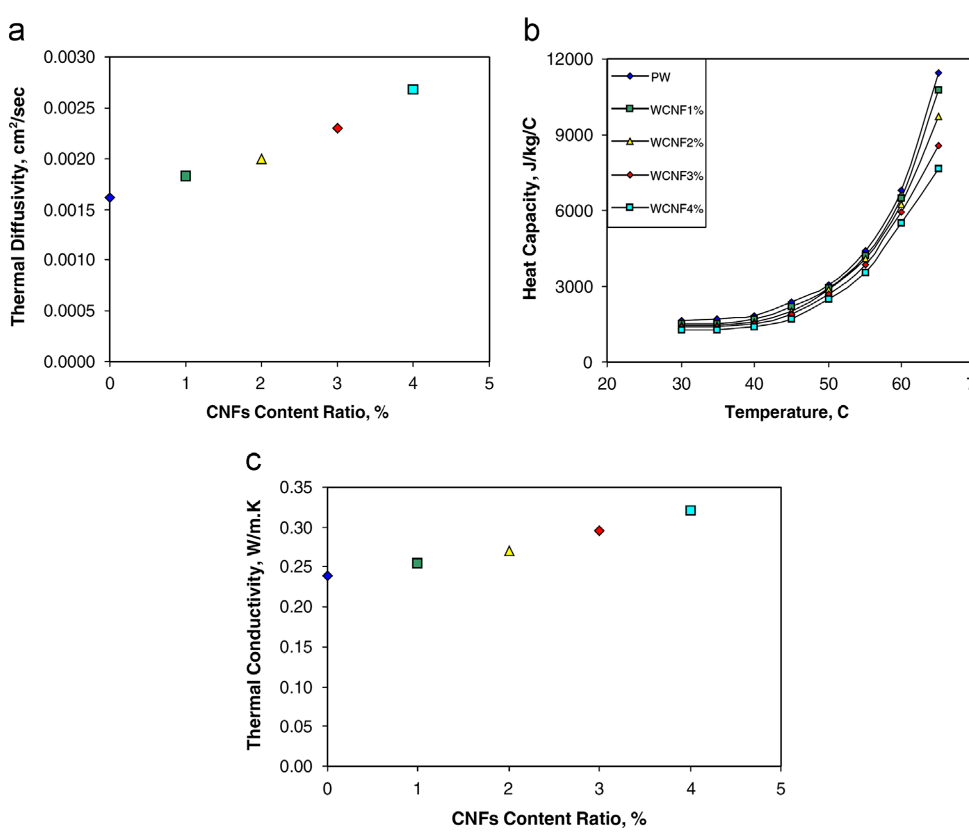


Fig. 3. Measured (a) thermal diffusivity at room temperature, (b) temperature-dependent specific heat capacity, and (c) thermal conductivity at room temperature for samples with different mass fractions of carbon nanofibers [17].

measured by recording the output of multiple type K thermocouples. The faster decay of the temperature data vs. time for nanofiber-loaded composites in comparison to pure paraffin (Fig. 4) pointed to the enhanced heat exchange properties of the samples. Predictions of the effective thermal conductivity of the composites using an analytic model agreed well with experimental data. Thermal performance of mixtures containing electrochemically treated nanofibers was found to be enhanced in comparison to composites with untreated fillers.

Recognizing the potential for a beneficial role of nanotechnology in thermal energy storage applications, Khodadadi and Hosseinizadeh [18] proposed an improved functionality of phase change materials through dispersion of high thermal conductivity nanoparticles in PCM. The resulting colloidal systems that were termed nanoparticle-enhanced phase change materials (NePCM) exhibited enhanced thermal conductivity in comparison to the base PCM. Focusing on a computational analysis, a water/copper nanoparticle (diameter of 10 nm) representative mixture was studied. Starting with steady-state natural convection within a differentially-heated square cavity that contained the NePCM of interest (vol% being 10 and 20), the solidification process of the colloidal suspension was studied. Due to increase of thermal conductivity, despite lowering of the latent heat of fusion, high heat release rate of the NePCM in relation to the base PCM was observed (Fig. 5). The mixture with a loading of 20% was observed to freeze in less than half the time period it took for the pure PCM.

Hong et al. [19,20] explored the influence of carbon nanotubes dispersed in liquids on lowering the freezing temperature of the resulting suspensions. Two types of single-walled nanotubes (SWNT) differing in impurities and level of fluorination were obtained from Carbon Nanotechnologies Inc. (Houston, TX). The base liquids were 50/50 mixtures of water with ethylene glycol (EG) available from Sigma Aldrich and a commercially available prediluted antifreeze coolant (PAC). Sodium dodecylbenzene sulfonate (SDBS) was used as the surfactant. Applying sonication, the nanotubes were dispersed in the base liquids (0.05, 0.1 and 0.2 wt%) and their stability was confirmed visually with the naked eye. The liquids were frozen and their freezing temperatures were obtained using the ASTM D1177 standard test method. Upon thawing, the extent of sedimentation or agglomeration was confirmed visually. The samples were found to remain

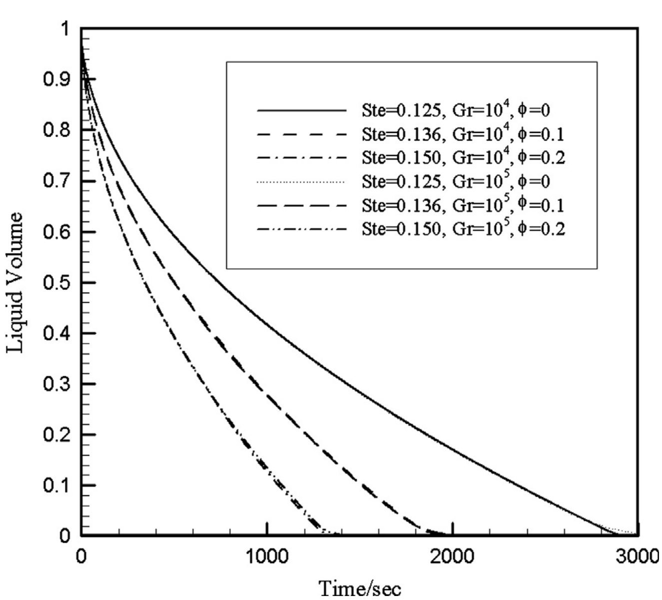


Fig. 5. Instantaneous variations of the liquid volume fraction during freezing processes of nanoparticle-enhanced phase change materials in a square cavity [18].

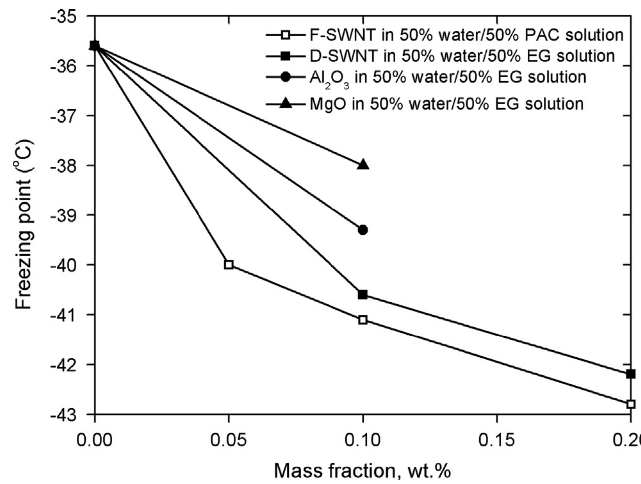


Fig. 6. Dependence of the freezing point of PAC and EG mixtures on mass fraction of the suspended enhancers [19,20].

stable in air for more than 1 month. The dependence of the measured freezing temperature on the weight percentage of the nanotubes is highlighted in Fig. 6 for both 50/50 water/PAC and water/EG-based liquids hosting F-SWNT and D-SWNT nanotubes, respectively. The presence of the dispersed nanotubes contributed noticeably to lowering of freezing point by about 7 °C for the highest loading. The pH values were also shown to have little effect on the measured freeze point. Limited freezing point data were also obtained by Hong et al. [20] were also obtained for 0.1 wt% Al_2O_3 and MgO nanoparticles (Sigma Aldrich) dispersed in 50/50 water/EG (Fig. 6). Similar trends but less pronounced in comparison to the nanotube-based mixtures were observed. The colligative property of the "solution" was identified for the noticeable lowering of the freezing temperature.

Zeng et al. [21] reported on in situ preparation of a 1-tetradecanol/Ag particle colloidal system through mixing and vigorous stirring of two intermediate solutions. The reported mass fraction of the silver particles ranged between 0.02 and 0.94. Communication with the authors clarified that at such high loadings the mixtures were not form-stable and exhibited fluidity upon heating and melting. The DSC-measured values of heat of fusion varied linearly with the loading of the particles, whereas the phase change temperature was lower in comparison to the pure PCM (MT of 38 °C and latent heat of 230 J/g). The claim to nanoparticle size of the suspensions appears to be questionable since the measured particle size was about 500 nm that is more than 1 order of magnitude greater than the accepted range for nanoparticles. The reported thermal conductivity enhancement with increased loading of Ag particles was not directly measured using accepted techniques. Instead, this was inferred from faster-rising reading of a thermocouple placed within a small sample of the solid composites while being heated from 0 to 33 °C. Exposure of the mixtures to two heating cycles (−30 to 70 °C at a rate of 10 °C/min) was deemed appropriate for claiming thermal stability of the composites.

Phase transformation temperatures of alumina and titania nanoparticles suspensions in deionized water prepared by a two-step technique that involved intense sonication and further homogenization by magnetic force agitation was investigated by Xie et al. [22]. The TiO_2 nanoparticles with an average diameter of 3.8 nm that were prepared in-house exhibited severe aggregation upon dispersion in water. Commercial γ phase Al_2O_3 nanoparticles (unknown source) that were used had an average diameter of 8 nm. The lowest/highest reported mass percentages for alumina and titania nanoparticles were 1.54/6.19 and 2.616/7.85%,

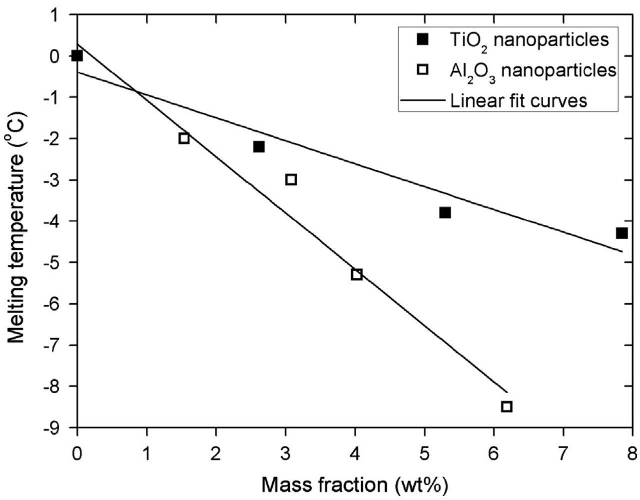


Fig. 7. Variation of the melting temperature as a function of mass fraction of nanoparticles for two different aqueous nanofluids [22].

respectively. The observed linear dependence of the melting temperature on the mass fraction of the nanoparticles is shown in Fig. 7, exhibiting a lowered melting temperature by 8.5 and 4 °C for the highest alumina and titania loadings, respectively. An analogy of the behavior of these colloidal suspensions to that of a dilute solution was implied and it was suggested that the observed difference of the melting point is determined to a lesser degree by the size of the particles and more by the adsorbability of the nanoparticles to the solvent molecules.

Graphite nanofibers (GNF) with diameters of 4–10 nm and lengths of up to 1 μm as verified by transmission electron microscopy (TEM) were prepared in-house by Weinstein et al. [23] and mixed with paraffin (melting temperature of 56 °C, C_p of 2.1 kJ/kg K, heat of fusion of 234 kJ/kg and thermal conductivity of 0.25 W/mK). Three styles of nanofibers identified as ribbon, platelet and herringbone were prepared through the catalytic deposition of hydrocarbon and/or carbon monoxide over metal catalysts. Among the three styles that featured solid metal catalysts in the middle and fibers grown on that particle, the herringbone fibers exhibited strong tendency to interconnecting that often led to a spongy agglomeration of particles. Mixtures of PCM/GNF with weight percentages of 0.25, 0.5, 1 and 5 were sonicated for 4 h. A cubic module of inside dimension of 5.08 cm with a hot bottom surface (made of copper and heated by a Kapton resistance heater), a cold top surface (kept at 5 °C by a circulating 50/50 water/antifreeze mixture) and low-conductivity acrylic/PVC side walls was used for melting experiments. The module that was also instrumented with 5 type T thermocouples was encased using fiberglass insulation. At the conclusion of sonication, the molten samples were poured gently into the cubic module and allowed to solidify. After each melting test, re-melting of the samples was preceded by resonication since significant settling was evident after three melting/freezing cycles without sonication. Exploring additives to prevent fiber settling was a concern but no information was provided. Heat capacity and thermal conductivity were measured for the solid phase using DSC and steady-state heating of a 100 cc instrumented solid block, respectively. The samples exhibited thermal conductivity enhancement as high as 2 orders of magnitude for the 5 wt% samples with ribbon and platelet GNF, however, the measured heat capacities showed little sensitivity to the presence of GNF additives and no data on heat of fusion was provided. Based on thermocouple readings at various heights within the melting module, pure PCM system was fully melted whereas for low fiber loadings, even though the GNF/PCM was effective in conducting heat, sizeable portion did not melt. The thermal performance was also found to be fiber style-dependent. As the fiber loading increased, thermal response improved however for significantly high fiber loadings, the Rayleigh–Benard convection currents were suppressed.

Being aware of the difficulties associated with uniform dispersion of carbon nanotubes in the liquid phase of PCM, Zeng et al. [24] reported on the preparation of form-stable composites via in situ polymerization. With 1-tetradecanol (TD) as the PCM (MT of 35 °C), polyaniline (PANI) served as the supporting material of the composite. Multi-walled nanotubes (MWNT) with an outer diameter of 10–30 nm and length of 5–15 μm were obtained from Shenzhen Nanotech Port Co., Ltd (Shenzhen, China). Composites with MWNT mass fractions of 0.5, 1, 2.5 and 5% were subjected to scanning electron microscope (SEM), thermogravimetry (TG/DTG) and DSC (−10 to 80 °C at a rate of 10 °C/min in N_2 environment), whereas their thermal conductivity at room temperature was obtained using the transient plane source technique (HotDisk Thermal Constants Analyzer, HotDisk AB, Gothenburg, SWEDEN). Upon heating of these *solid* samples above the melting temperature of the PCM to 80 °C, the original shapes were retained and no liquid traces were observed. DSC measurements of the PCM (TD), form-stable PCM (PANI/TD) and the PANI/TD/MWNT (5 wt%) composites are shown in Fig. 8. The phase change temperature was observed to be lower than the MT of TD by a couple of degrees, whereas the heat of fusion was not affected greatly upon introduction of the MWNT (lowered from 119.14 to 114.49 J/g). However, one should also note the noticeable decrease of the latent heat of the PANI/TD composite (about 50/50 by mass) in comparison to the pure TD. A linear enhancement of the measured thermal conductivity values of these form-stable solid composites was observed exhibiting 30% improvement for the 5 wt% sample.

Single-walled carbon nanotubes (SWCNT), multi-walled carbon NT (MWCNT) and carbon nanofibers (CNF) with nominal diameters of 1, 10 and 100 nm, respectively, were individually combined with paraffin wax, referred to as shell wax 100 (latent heat of 156.3 J/g), by Shaikh et al. [25]. The suppliers of these nanomaterials were not identified. Shear mixing by using ultrasonication and melting techniques were applied for 4 h for preparation of the 0.1, 0.2, 0.4, 0.7 and 1% volume fraction mixtures. Fluidity of the mixtures was implied based on visual observation that the wax/SWCNT suspensions exhibited “better dispersion” compared to the other two mixtures. Values of the latent heat of fusion of the mixtures were measured using DSC by subjecting the samples to two melting-freezing cycles. Upon introduction of additives, melting temperature of the mixtures was observed to rise slightly in the 0.4–1 °C range in comparison

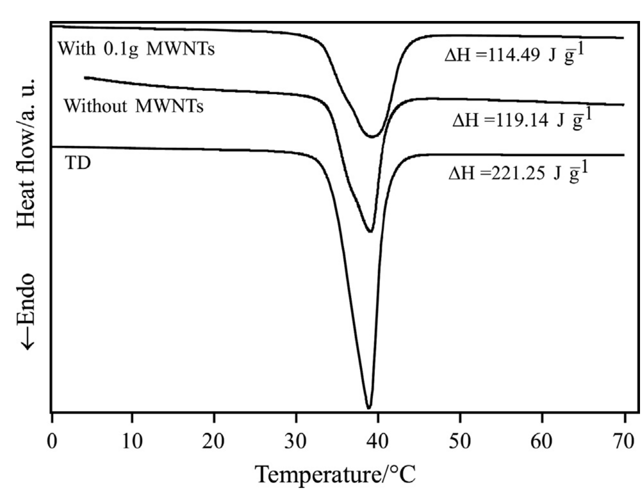


Fig. 8. Comparison of DSC curves for pure 1-tetradecanol (TD), form-stable composite with TD and polyaniline, and composite enhanced by adding 5 wt% multi-walled carbon nanotubes [24].

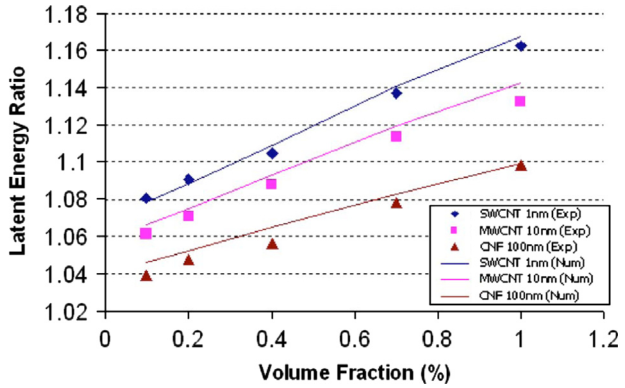


Fig. 9. Comparison of predicted and measured latent heat of fusion of the mixtures with different additives [25].

to the base PCM. The dependence of the measured values of the heat of fusion on the volume fraction of the additives for the three types of mixtures is given in Fig. 9. The anomalous rise of heat of fusion is registered for all the samples with the greatest enhancement level being 16% for the 1 vol% wax/SWCNT mixtures.

Owing to their low density and high thermal conductivity, 95% purity multi-walled carbon nanotubes (Chengdu Organic Chemicals Co., Ltd., Chinese Academy of Sciences) and 98% palmitic acid (PA) (density of 853 kg/m^3, MT of 62.5–64 °C and latent heat of 207.8 J/g) supplied by Sinopharm Chemical Reagent Co., Ltd, Shenzhen, China, were combined by Wang et al. [26] to form the main components of a PCM/CNT mixture. The average diameter, average length and specific surface area of the CNT were 30 nm, 50 μm and 60 m^2/g, respectively. In order to promote their dispersibility, the CNT were subjected to chemical treatment with a 1:3 concentrated nitric/sulfuric acid mixture that entailed boiling, refluxing, dilution with distilled water and filtration. Upon drying at 100 °C for 24 h, the CNT powder was added to melting PA and the mixture was then subjected to intensive sonication. Samples with mass fractions of 0.5, 1, 2 and 5% were studied using SEM and their thermal conductivity was measured using the transient short-hot-wire technique (uncertainty less than 0.5%) that utilized a platinum wire (diameter of 70 μm). The melting temperature and latent heat were determined using DSC that was operated twice in the temperature range of 15–110 °C at a heating rate of 5 °C/min. Stability of the composites was tested by exposing the samples to 80 consecutive cycles of heating in an oven (12 h) and cooling to room temperature (2 h) with the oven temperature equal to 70 °C (> MT of PA). The samples were then cut and photographed. Observed homogeneity and lack of coagulation of CNTs led the authors to declare the samples stable. The thermograms that were obtained using DSC exhibited shifts of phase transition peaks due to addition of CNTs. The lowering of the melting temperature and latent heat as functions of mass fraction are observed in Fig. 10, which is in concert with findings of previous investigations, except Shaikh et al. [25]. The predicted latent heat using the theories of mixtures is also given in Fig. 10 and the lower measured values were attributed to the interaction forces between PA and the CNT surfaces. The variations of the measured thermal conductivity of the mixtures as a function of the temperature of the sample are given in Fig. 11. It should be noted that this is the first paper in which detailed thermal conductivity data in both phases are presented. At a given temperature, the thermal conductivity is consistently raised upon addition of the CNTs. For a narrow temperature range of about 10 °C centered about the melting temperatures of the mixtures, an abrupt rise of thermal conductivity in the solid phase followed by a sharp decline is measured, whereas on the both sides of this range, the thermal conductivity exhibits extremely mild sensitivity

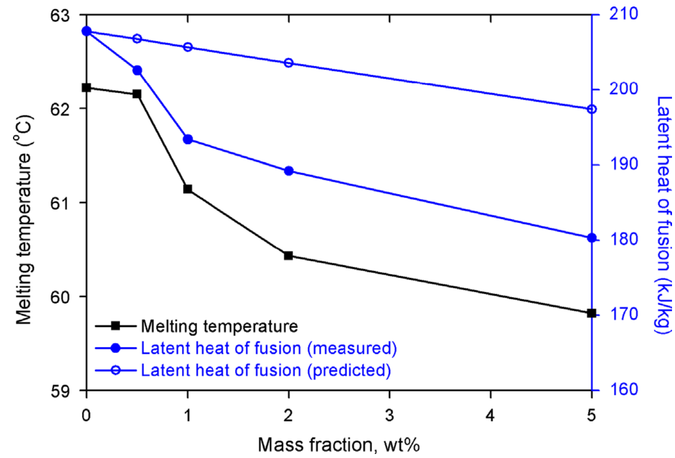


Fig. 10. Measured melting temperature along with measured and predicted latent heat of fusion of the mixtures for various weight fractions of the additives [26].

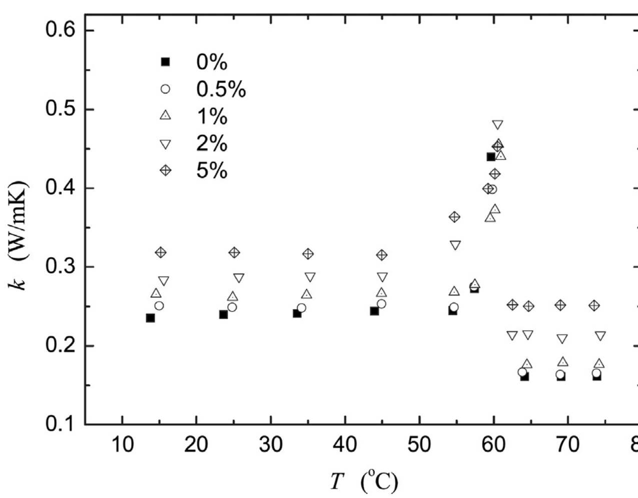


Fig. 11. Measured temperature-dependent thermal conductivity of the mixtures in both phases for various weight fractions of the additives using the THW technique [26].

to temperature variation. The thermal conductivity of the solid phase is consistently higher than the value measured for the same sample in its liquid state. Whereas the thermal conductivity enhancement index was found to be independent of temperature for the 0.5 and 1 wt% samples, an incremental jump was registered for the 2 and 5 wt% samples upon melting.

In order to examine the effect of exfoliated graphite nanoplatelets (xGnP™) on enhancing electric conductivity, thermal conductivity and latent heat storage of phase change materials, 1, 2, 3, 5 and 7 wt% mixtures of paraffin/xGnP were prepared by Kim and Drzal [27]. The paraffin wax was *n*-docosane (Sigma Aldrich with melting temperature of 53–57 °C, thermal conductivity of 0.26 W/mK and latent heat of 157.3 kJ/kg), whereas xGnP was prepared starting from sulfuric acid-intercalated expandable graphite (Asbury Graphite Mills, Inc., Asbury, NJ). Processing of graphite resulted in nanoplatelets with an average diameter of 15 μm and thickness being less than 10 nm (surface area of 30 m^2/g) that were then mixed with liquid paraffin at 75 °C, filtered and dried. The solid samples were re-melted into a mixture to be processed for electrical and thermal conductivity measurements. Specifically, 1 in. diameter and 5 mm thick specimen were molded and thermal conductivity was measured at 20 °C under an applied load of 30 psi using the ASTM E1530 standard (guarded heat flow meter technique). Thermal energy storage properties were obtained

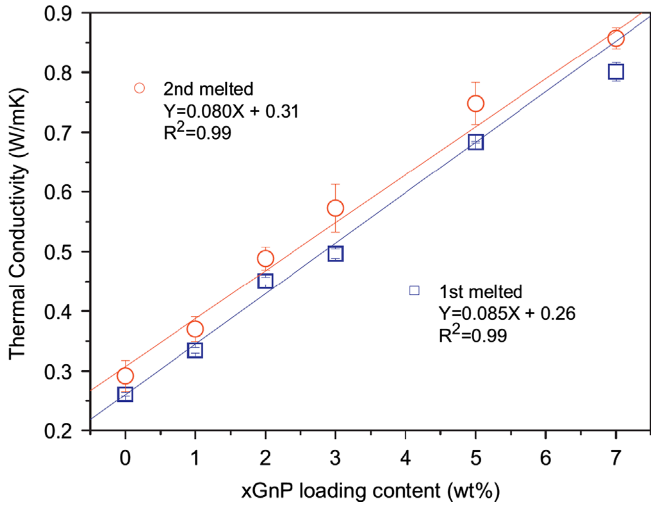


Fig. 12. Measured thermal conductivity of the paraffin/xGnP PCM composites as a function of the loading of xGnP using the steady-state method [27].

using DSC (−50 to 110 °C at a rate of 10 °C/min in N_2 environment) after the samples were quickly cooled to −50 °C from the melt of the first scan. Scanning electron micrographs exhibited uniform dispersion of nanoplatelets in paraffin. The measured thermal conductivity of pure paraffin and paraffin/xGnP composites at 20 °C are shown in Fig. 12 exhibiting a linear dependence on the mass fraction of the nanoplatelets. The samples that were re-tested after melting and re-casting also exhibited similar trends for thermal conductivity enhancement. Two phase change peaks were observed in the melting and freezing DSC curves for pure paraffin and paraffin/xGnP specimen (shown in Fig. 13 for pure and 5 wt% samples). The peak at the lower temperature is related to solid–solid transition, whereas the one at the higher temperature is indicative of the solid–liquid phase change. Surprisingly, the latent heat values obtained by numerical integration of these curves about the two peaks did not indicate the expected diminished value of heat of fusion due to replacement of the PCM with dispersions.

Starting with pristine long and short (P-L and P-S) multi-walled nanotubes (Shenzhen Nanotech Port Co., Ltd, Shenzhen, China) with lengths of 5–15 and 1–2 μm, respectively, and outer diameter of 10–30 nm, Zeng et al. [28] applied an involved surface oxidation process by nitric acid (O-L and O-S) and a 50/50 nitric/sulfuric mixture acid (M-L and M-S). In effect, six variations of MWNT were available. Palmitic acid (PA) (MT of 59.48 °C, freezing temperature (FT) of 58.78 °C and latent heat of 201 J/g) served as the base PCM. PCM/MWNT systems were obtained by mixing PA, surfactants (if needed) and the respective MWNT in capped test tubes and applying ultrasonication at 80 °C for 1 h. Two surfactants, SDBS and cetyltrimethyl ammonium bromide (CTAB), were used. Upon cooling to room temperatures, the samples were grinded. In preparing all samples, 2 g of PCM and 0.1 g of a surfactant (if needed) were used. Fifteen samples with P-L MWNT were prepared by mixing 0.002, 0.01, 0.02, 0.04 and 0.1 g with PCM, PCM/CTAB and SDBS. The mass percentages for five surfactant-free samples were 0.099, 0.5, 1, 1.96 and 4.76, whereas for the remaining ten samples with the two surfactants the weight percentages were 0.095, 0.47, 0.94, 1.87 and 4.5. Fifteen other samples utilizing P-S, O-L, M-L, O-S and M-S MWNT were prepared matching the highest mass fractions of the P-L samples. The MWNT were subjected to a Fourier transform infrared spectrometer, whereas energy storage properties were obtained using DSC (20–100 °C at a rate of 10 °C/min in N_2 environment). Thermal conductivities of ground samples at room temperature

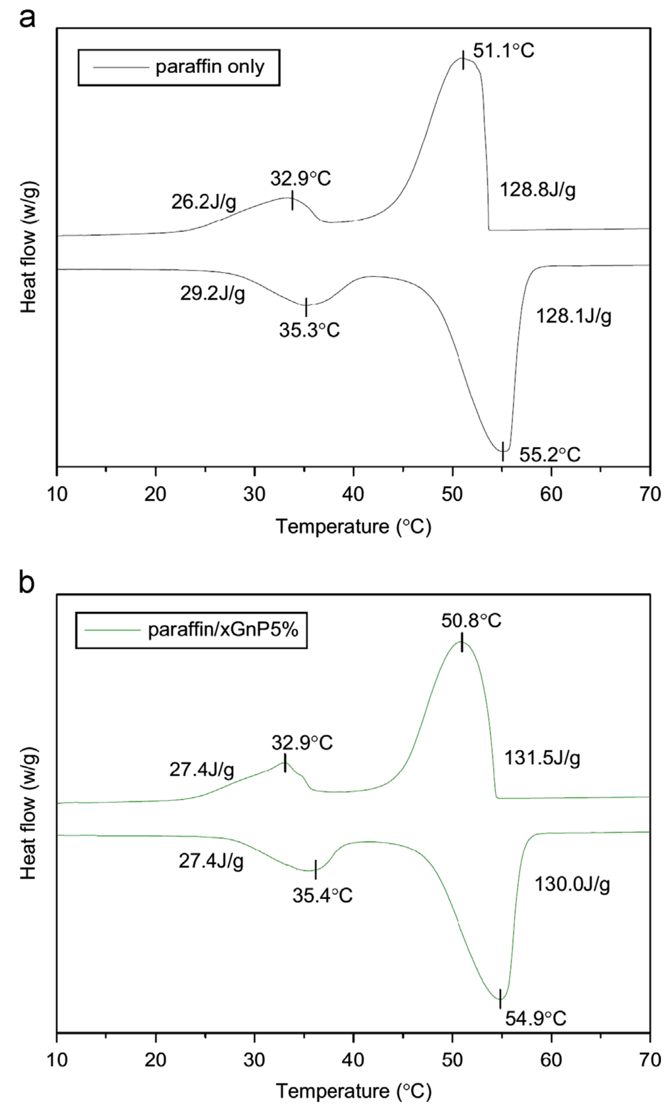


Fig. 13. DSC melting and freezing curves of (a) pure paraffin (*n*-docosane) and (b) paraffin/xGnP mixtures with 5 wt% xGnP [27].

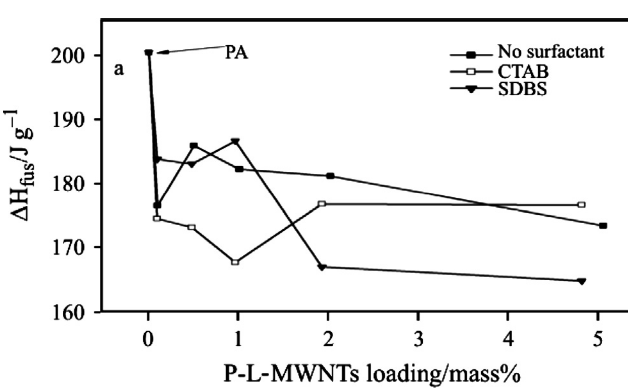


Fig. 14. Comparison of the latent heat of fusion of the mixtures as a function of mass fraction of the added pristine long multi-walled carbon nanotubes (PL-MWCNT) with different surfactants [28].

were obtained using the transient plane source technique (Hot-Disk Thermal Constants Analyzer, Hot Disk AB, Gothenburg, SWEDEN). This involved forming two cylinders (diameter of 13 mm) upon pressing the samples under 20 MPa. The measured heat of fusion of the P-L samples are shown in Fig. 14. For low values of the MWNT loading, the heat of fusion drops abruptly

reaching a minimum. As the loading is increased, the heat of fusion recovers and attains a local maximum. The nanotube loadings corresponding to the observed maxima were dependent on the surfactant or lack it. With no surfactant, this loading was 0.5 wt%, whereas with SDBS and CTAB, the loadings were 1 and 2 wt%, respectively. For greater loading of the CNT, a linear decline of the measured values of heat of fusion was observed. The minima and maxima were attributed to the greater uniformity of dispersion (thus greater absorption of PA by nanotubes) and agglomeration of nanotubes, respectively. The effect of surface oxidation and length of the MWNT on the observed values of the heat of fusion for a nearly constant loading of about 5 wt% are illustrated in Fig. 15. No noticeable trends in relation to the length of the nanotubes were observed, whereas the surfactant-treated samples exhibited a lower value of heat of fusion. The long

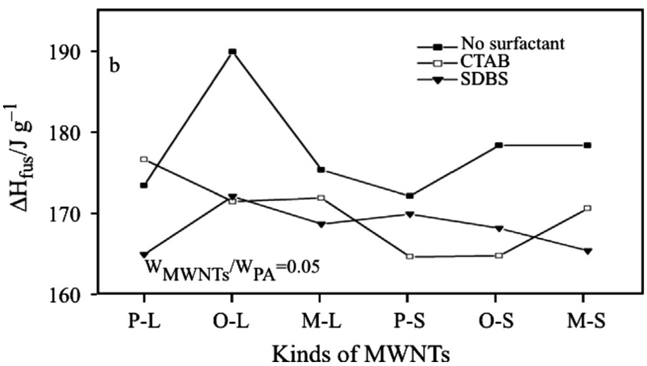


Fig. 15. Comparison of the latent heat of fusion of mixtures with different types of added MWCNT for a mass fraction of 5 wt% [28].

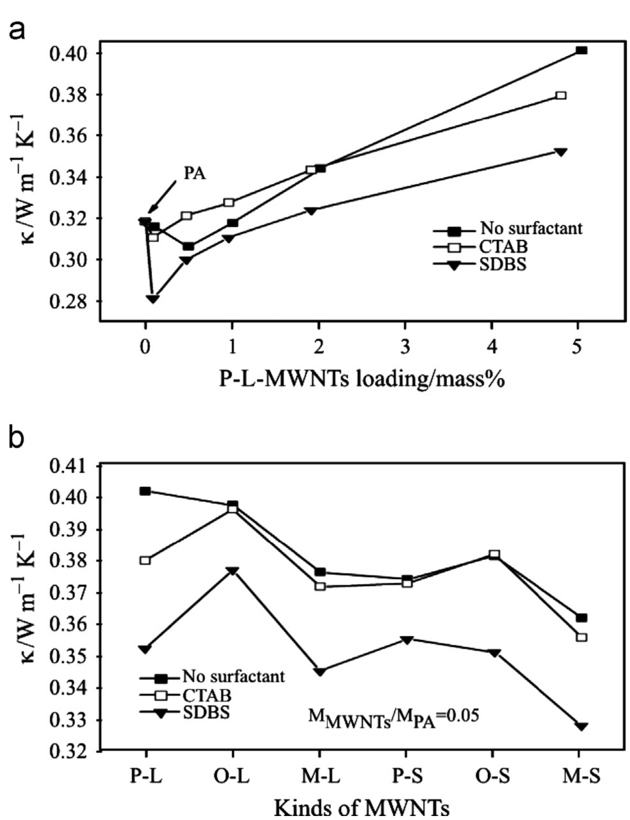


Fig. 16. Comparison of the measured thermal conductivity of the solid composites at room temperature for (a) different mass fractions of the added pristine long MWCNT, and (b) different kinds of MWCNT for a mass fraction of 5 wt%, using the TPS method [28].

nanotube sample treated with HNO_3 exhibited the highest value of heat of fusion owing to weaker oxidizability by nitric acid in comparison to the mixed acid and greater resistance of long nanotubes to oxidation. Thus, fewer active groups on the surface of O-L nanotubes are expected in comparison to other acid-treated samples. The measured values of the thermal conductivity of the P-L samples plotted against the loading and type of the nanotubes are shown in Fig. 16a and b, respectively. For low loading of MWNT, the thermal conductivity is smaller than pure PA (0.318 W/mK), owing to high interface thermal resistivity (lack of a conductive network). Presence of the surfactants compounded this effect to some extent. Upon introduction of greater number of nanotubes, the measured thermal conductivity values began to rise linearly against the mass fraction of the nanotubes. For loadings of the P-L samples above 2 wt%, the presence of the surfactants did not have a positive role on enhancing the thermal conductivity. As for the effect of the length of the nanotubes and surface treatment on thermal conductivity (Fig. 16b for 5 wt%), the longer nanotubes contributed to greater enhancement. Greater enhancement exhibited by the CTAB-treated samples compared to SDBS was attributed to the greater ability of CTAB to disperse the nanotubes more evenly.

Liu et al. [29] dispersed titanium oxide nanoparticles in saturated $BaCl_2$ (FT of −8 °C) aqueous solution with a pH of 8.

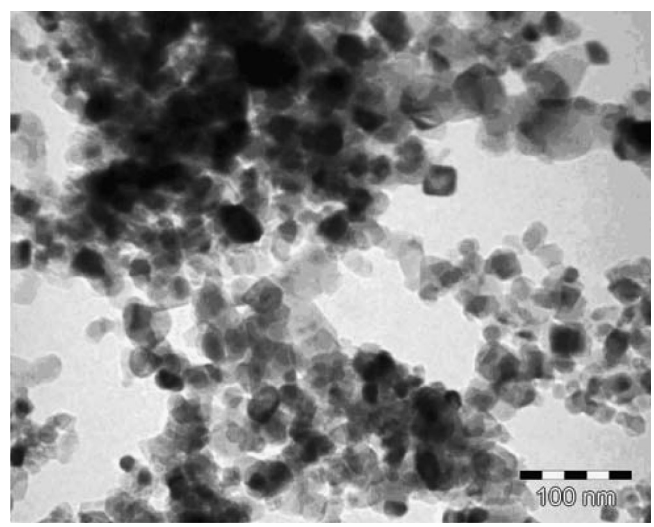


Fig. 17. TEM image of the titanium oxide (TiO_2) nanoparticles showing a nominal diameter of 20 nm [29].

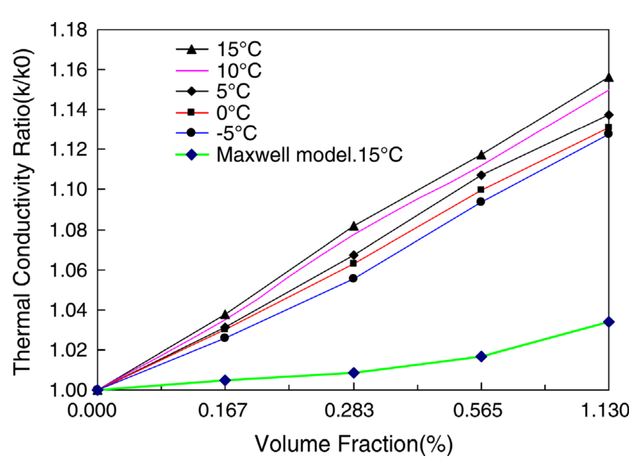


Fig. 18. Measured thermal conductivity ratio of the nanofluids as a function of volume fraction of nanoparticles at various temperatures using the THW method [29].

TEM images of the TiO_2 nanoparticles that have a mean diameter of 20 nm are shown in Fig. 17. Utilization of a supersonic oscillator helped to improve the dispersion of the nanoparticles, whereas no thickening agents were used. The volume loadings of the mixtures were 0.167, 0.283, 0.565 and 1.13%. The transient hot wire technique utilizing a Teflon-coated pure platinum wire was used for measuring the thermal conductivity. The normalized thermal conductivity ratios at various temperatures above the freezing temperature (−8 °C) are plotted against the volume fraction in Fig. 18 along with the theoretical prediction of the model proposed by Maxwell [5]. At a given temperature, the measured thermal conductivity rises linearly with the volume fraction, whereas thermal conductivity also exhibits a clear rising trend with temperature for a given volume fraction (not supported by the liquid phase data of Wang et al. [26]). The predicted value of the thermal conductivity due to Maxwell′s model is noticeably lower than the measured quantities. The performance of the $BaCl_2$–H_2O–TiO_2 composite (1.13 vol%) during charge/discharge portions was studied by utilizing the PCM in a cool storage/supply unit. The temperatures of the PCM with and without nanoparticles during the freezing and thawing experiments are shown in Fig. 19a and b, respectively. The enhanced performance of the PCM/colloid system that is brought about by its increased thermal conductivity and exhibited by lowering of the charge/discharge time periods is clearly observed. Moreover, during the freezing experiments, the nanoparticles are observed to act as nucleating agents and reduce supercooling. System-level enhancements of the values of the cool storage/supply rate and capacity were also noted.

Spherical alumina nanoparticles (Alfa Aesar, Ward Hill, MA) with an average diameter of 20 nm were dispersed in a double-distilled water/SDBS mixture and then subjected to ultrasonication (40 kHz) for 1 h at room temperature by Wu et al. [30]. SDBS (Guangzhu Chemical Reagent Factory, China) was the dispersant agent of the colloids with alumina weight fractions of 0.0005, 0.001 and 0.002 (1:1 by weight of alumina and SDBS). A commercial transient hot wire instrument utilizing a 10 μm nickel-based wire was used for measuring the thermal conductivity. The reported thermal conductivity values for 0, 0.05, 0.1 and 0.2 wt% samples were 0.6008, 0.6483, 0.6525 and 0.6639 W/mK, respectively. Distribution of the particle sizes in the absence and presence of the dispersant for a 0.2 wt% colloid is shown in Fig. 20a and b, respectively (technique was not specified but most probably it is dynamic light scattering). The corresponding average particle sizes were 433 and 259 nm, indicating that the presence of dispersant SDBS was helpful in lowering the level of agglomeration of the 20 nm particles. High absolute values of the measured zeta potential (greater than 30 mV) were reasoned to

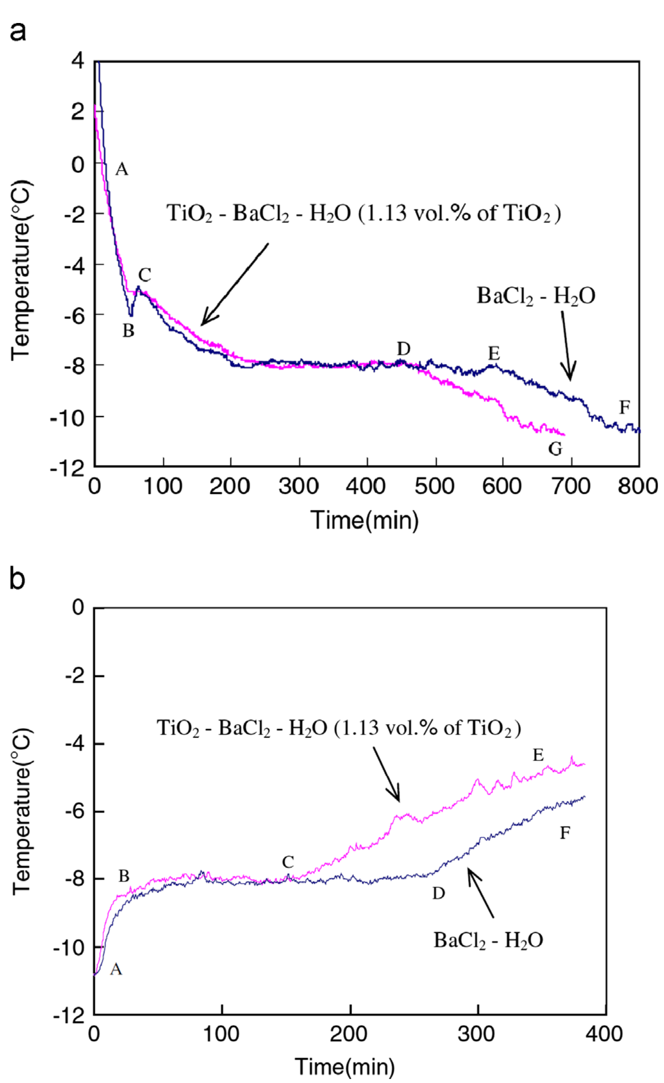


Fig. 19. Time histories of temperature during (a) freezing and (b) thawing processes for the 1.13 vol% nanofluid in comparison to those of the base liquid [29].

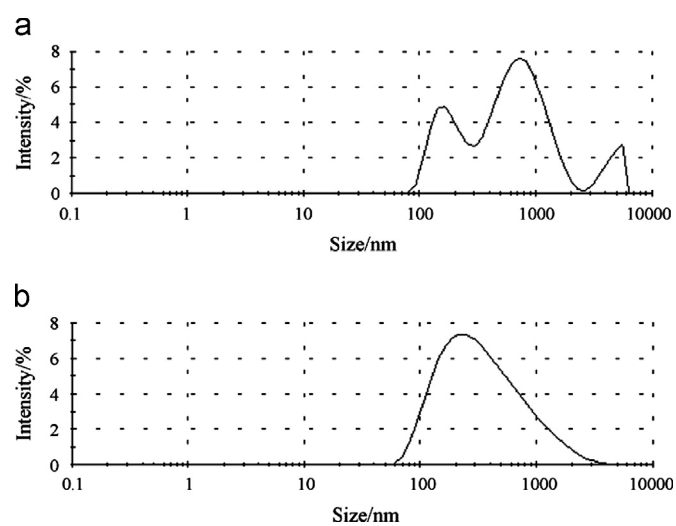


Fig. 20. Comparison of the particle size distributions of the alumina-water nanofluids for samples (a) without and (b) with SDBS dispersant [30].

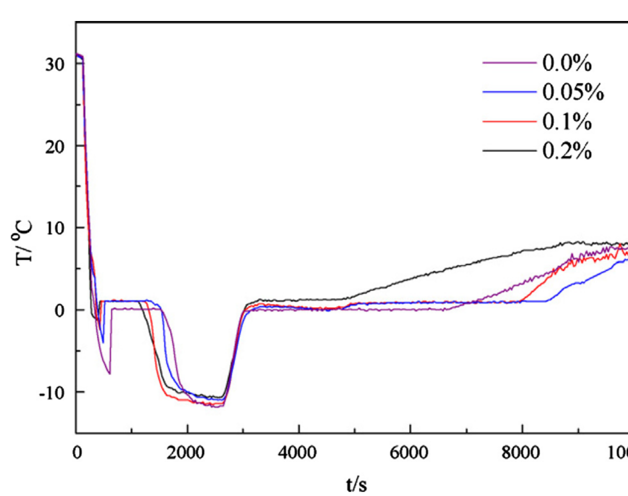


Fig. 21. Time histories of temperatures of the alumina-water nanofluids with different mass fractions during a freezing process [30].

be an indication of the stability of the colloid. An experimental thermal response test section utilizing a 1:1 water and glycol mixture was utilized. Test tubes filled with colloidal samples were placed in the test section and subjected to a cool-down period to −20 °C followed by a heat-up period to 15 °C. Monitored transient temperature data of the samples (Fig. 21) indicated a realization of improvement of supercooling and shortening of the freezing time in response to greater concentration of the nanoparticles. The reported phase change temperature that was based on this crude experiment was observed to be independent of the fraction of nanoparticles. The colloidal samples (50 ml) were also placed in 150 ml beakers which were then placed in a −15 °C water–glycol bath and allowed to freeze. An infrared imaging instrument was utilized to monitor the freezing of the samples qualitatively. The infrared images of the samples after 10 and 36 min are shown in Fig. 22a and b, respectively. The 0.2 wt% composite exhibited a 20.5% reduced freezing time period.

Ho and Gao [31] prepared colloidal suspensions (5 and 10 wt%) of alumina nanoparticles (Nanotech, Kanto Chemical Co. Inc., Japan) in *n*-octadecane (99.9% pure $C_{18}H_{38}$, MT of 26.5 °C, FT of 25.1 °C and latent heat of 243.1 J/g, Zeeland Chemicals, USA). An unspecified non-ionic surfactant (1/3 of the desired mass fraction) was used to coat the nanoparticles followed by their dispersion in the liquid paraffin using sonication for a minimum of 3 h. Sonication was carried out in a constant-temperature bath that was kept above the melting point of the paraffin. Applying the laser diffraction technique to the colloidal samples, the volume–mean diameters of alumina particles were determined to be 159.6 and 196 nm corresponding to 5 and 10 wt% samples, respectively, whereas Gao [32] specified the average diameter of the particles to be 33 nm. This finding points to agglomeration of the nanoparticles similar to observations to Xie et al. [22] and Wu et al. [30]. Values of the freezing/melting temperatures and latent heat were obtained using DSC (temperature range of 20–40 °C at a rate of 2 °C/min). Density, dynamic viscosity and thermal conductivity of the samples were measured using a hydrometer (Tomei Co. Ltd, Japan, accuracy within $\pm 5\times10^{-4}$ g/cm^3), rotational viscometer (Brookfield DV-II+Pro, Middleboro, MA, standard deviation of less than ±1%) and transient hot wire technique (KD2 PRO Thermal Analyzer, Decagon Devices, Pullman, WA, standard deviation of less than ±5%), respectively. The effect of nanoparticles on the melting/freezing temperatures was not noticeable, whereas the heat of fusion was reduced by about 7 and 13% for the 5 and 10 wt % colloidal samples, respectively. The dependence of the density of the samples on temperature and mass fraction is presented in Fig. 23. The density of pure *n*-octadecane decreases as the temperature is raised and the measurements agree very well with the data reported by Humphries and Griggs [33]. Density of the

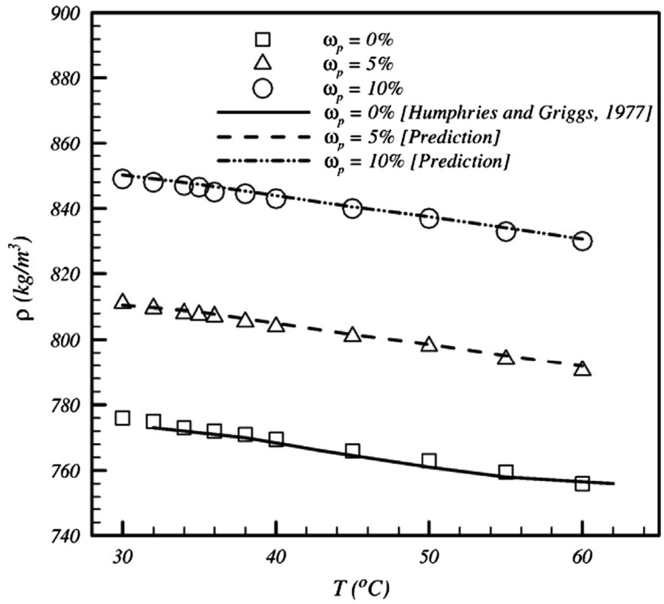


Fig. 23. Measured density for pure paraffin and nanoparticle-enhanced paraffin mixtures at various temperatures [31].

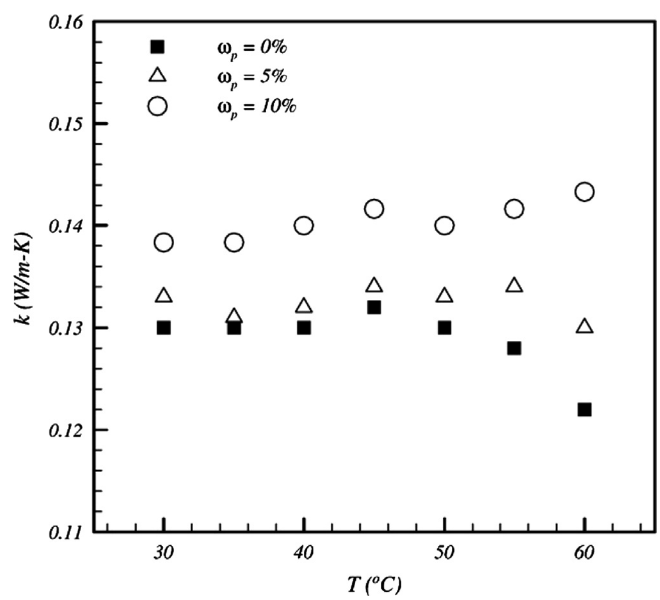


Fig. 24. Measured thermal conductivity for pure paraffin and nanoparticle-enhanced paraffin mixtures at various temperatures using the THW method [31].

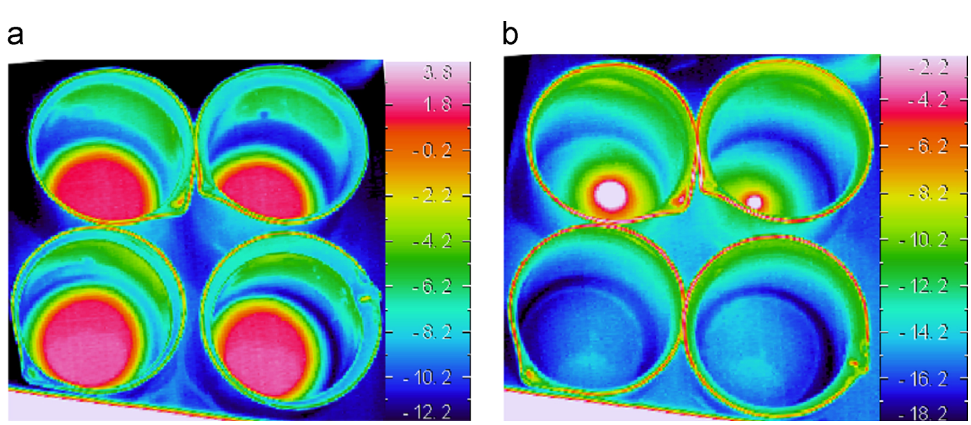


Fig. 22. Infrared temperature (unit: °C) images of the alumina-water nanofluids (particle loading increasing from left top to right bottom) at two instants ((a) $t=10$ min and (b) 36 min) during a freezing process [30].

two colloidal samples is also observed to follow a similar trend with temperature, whereas at a given temperature, the greater loading of the nanoparticles gives rise to a denser mixture. The experimental observations are also compared very favorably to predictions of the mixture theory that includes the contributions of the particles, surfactant and the base liquid. The measured values of thermal conductivity for different temperatures and mass fractions in the liquid phase of the PCM are given in Fig. 24. Thermal conductivity of pure *n*-octadecane in liquid phase between the melting temperature and about 50 °C is constant and then decreases upon further heating. The decaying trend of the thermal conductivity at high temperatures is well-documented [34]. At a given temperature, enhancement of thermal conductivity is consistently observed as the mass fraction was raised. The extent of enhancement was also observed to be greater at higher temperatures. The variations of the viscosity of the samples on mass fraction and temperature are presented in Fig. 25. As the temperature is raised, the viscosity of all the samples decrease monotonically and the measured viscosities for pure *n*-octadecane are in concert with data reported by Humphries and Griggs [33]. The extent of enhancement of viscosity of colloidal samples in comparison to enhancement of thermal conductivity for the same parameters is observed to be more marked. Melting experiments were carried out with these colloidal systems within a differentially-heated square enclosure [32]. The relevant parameters, i.e. the Rayleigh, Stefan and subcooling numbers, were 1.71×10^6–5.67×10^6, 0.037–0.108 and 0.042–0.537, respectively. It was concluded that buoyancy-driven convection in the melted zone and the effectiveness of the thermal energy storage tended to decrease greatly with increasing the mass fraction. The marked increase of viscosity due to the presence of nanoparticles, which significantly suppresses buoyancy-driven convection during melting outweighed the enhancement brought about by increase in values of thermal conductivity.

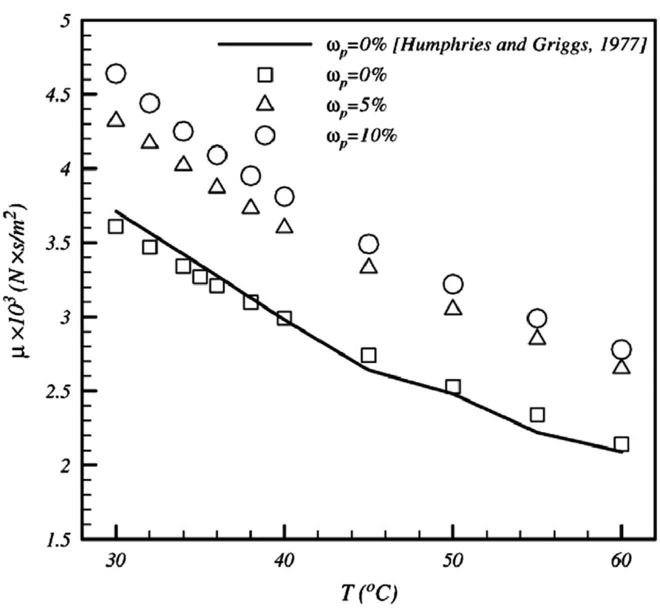


Fig. 25. Measured dynamic viscosity for pure paraffin and nanoparticle-enhanced paraffin mixtures at various temperatures [31].

In order to study the temperature-dependent thermophysical properties of PCM/MWNT mixtures, Wang et al. [35] combined 95% purity MWNT (Chengdu Organic Chemicals Co., Ltd., Chinese Academy of Sciences) and industrial grade paraffin wax (MT of 52–54 °C and latent heat of 165.3 J/g) supplied by Sinopharm Chemical Reagent Co., Ltd, Shenzhen, China. The average diameter, average length and specific surface area of the MWNT were 30 nm, 50 μm and 60 m^2/g, respectively. In order to promote dispersability of MWNT, these were cut by ball milling. SEM images of pristine and processed CNT after 12 h of application of ball milling are shown in Fig. 26a and b, respectively, showing that the treated MWNT appear shorter. The processed MWNT were then combined with molten paraffin and the mixtures were subjected to intensive sonication. Samples with mass fractions of 0.2, 0.5, 1 and 2 wt% were subjected to SEM and their melting temperature and latent heat capacity were determined using DSC (temperature range of 0–75 °C at a heating rate of 5 °C/min). Thermal conductivity of pure paraffin and mixtures was measured using the transient short-hot-wire technique (uncertainty estimated to be within ± 1%) that utilized a platinum wire (diameter of 70 μm). Samples were tested for their stability by keeping the samples in an oven at a temperature equal to 70 °C for 96 h. These samples were then

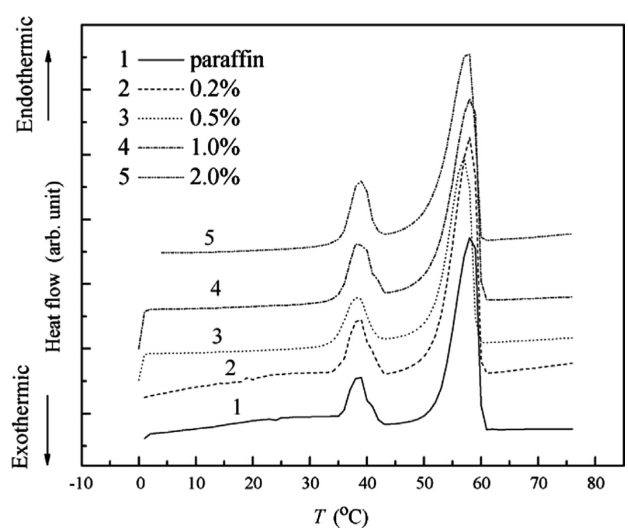


Fig. 27. Comparison of the DSC curves for pure paraffin wax and nanotube-enhanced mixtures with different loadings [35].

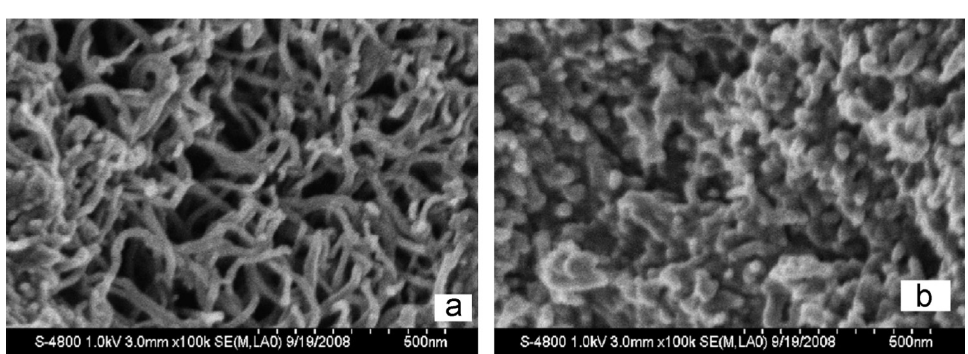


Fig. 26. SEM images for the (a) pristine and (b) treated multi-walled carbon nanotubes by ball milling [35].

removed, allowed to cool down to room temperature, cut and photographed in order to observe possible delamination. The samples were observed to be homogeneous and no delamination was detected. The DSC-based thermograms (Fig. 27) exhibited small peaks corresponding to solid–solid phase change and main peaks signifying solid–liquid phase change. Shifts of phase transition peaks are also observed as a result of addition of MWNT. Lowering of the melting temperature (about 1°) and latent heat was observed as the mass fraction was increased. However, the measured values of the latent heat were greater than the predicted latent heat using the theory of mixtures by a maximum of 1.8 kJ/kg. Dependence of the measured thermal conductivity of the mixtures on the temperature of the sample for both phases is given in Fig. 28. The presented data points are averages of 3 measurements and the thermal conductivity of the solid phase is consistently greater than the value measured for the same sample in its liquid state. For a given temperature, the value of the thermal conductivity is consistently increased as the mass fraction of the MWNT is raised. For a constant value of the mass fraction, whereas the thermal conductivity is found to be a weak function of temperature for values below 40 and above 55 °C, an abrupt rise of thermal conductivity is observed for pure paraffin, 0.2 and 0.5 wt% samples near the melting temperature. The reason behind this was not clear and further investigation based on molecular dynamics simulations was mentioned to be underway. Over a narrow temperature range of about 6 °C centered about the melting temperatures of the colloidal systems, a sharp decline of thermal conductivity was observed. Lowering of the intramolecular forces and formation of the disorderly liquid state upon melting were identified for this behavior. Thermal conductivity enhancement index did not exhibit a specific dependence on temperature; however, a clear rising trend with increasing of the mass fraction was observed, with as much as 35% rise for the 2 wt% sample. The important role of thermal resistance at the interface of the paraffin and MWNT was discussed in relation to the measured values.

Zeng et al. [36] prepared form-stable composites of 1-tetradecanol/Ag nanowires through ultrasonication of an anhydrone ethanol mixture at 343 K over periods of 10 min and 1 h with an intermediate cool-down/ethanol evaporation period. Upon final cool-down and drying in vacuum at room temperature for 24 h, it was ground. Silver nanowires with an outer diameter of 10–30 nm and length of 5–15 μm were obtained from Shenzhen Nanotech Port Co., Ltd (Shenzhen, China). Mixtures with Ag nanowire mass percentages of 9.09, 23.08, 37.58, 46.08 and 62.73 were subjected to SEM, XRD, TG, IR Spectroscopy and DSC (0–60 °C at a rate of 10 °C/min in N_2 environment). Thermal conductivity at room temperature was obtained using the transient plane source technique (HotDisk Thermal Constants Analyzer, Hot Disk AB, Gothenburg, Sweden) using two cylinder samples (diameter of 13 mm) pressed under 20 MPa. The DSC-measured heat of fusion of the mixtures that are presented in Fig. 29 varied linearly against the mass fraction of the silver nanowires. The values of the thermal conductivity of the mixtures at room temperature are plotted against the mass fraction of the silver nanowires in Fig. 30. Linear dependence of thermal conductivity over two ranges of the mass fraction (0–40 wt% and 40–70 wt%) is observed. Comparing properties of their form-stable composites to those of metal powder-filled solid composites, the enhanced thermal conductivity was attributed to the high aspect-ratio of the silver nanowires. The authors also observed greater enhancement of the thermal conductivity afforded by the silver nanowires in comparison to MWNT/TD-based composites developed by their group [24,28].

Wang et al. [37] applied a mechano-chemical process in order to treat the surfaces of multi-walled carbon nanotubes in order to enhance their dispersability. Pristine MWNT (Chengdu Organic Chemicals Co., Ltd., Chinese Academy of Sciences with average diameter, average length and specific surface area of the CNT were

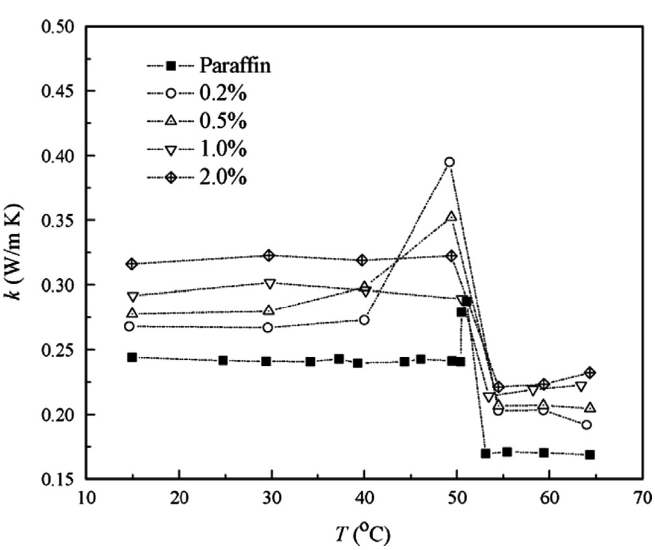


Fig. 28. Temperature-dependent thermal conductivity of pure paraffin wax and nanotube-enhanced mixtures for both solid and liquid states using the THW method [35].

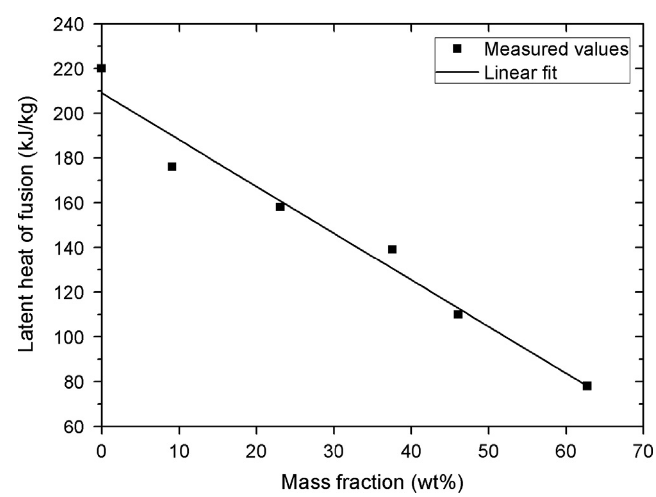


Fig. 29. Variation of the measured latent heat of fusion of the composites as a function of the mass fraction of silver nanowires [36].

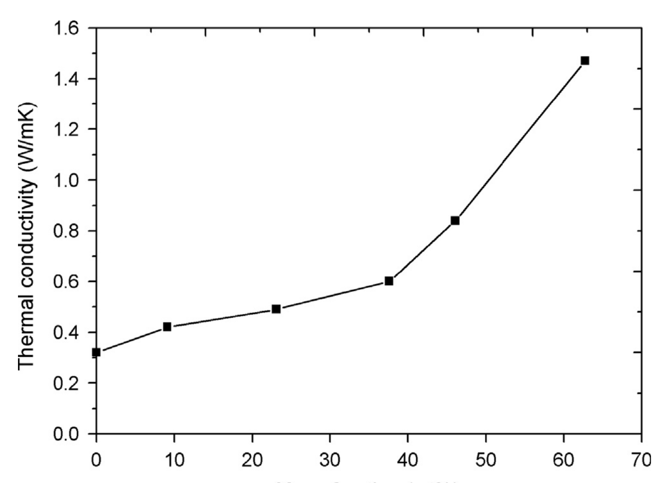


Fig. 30. Variation of the measured effective thermal conductivity of the composites as a function of the mass fraction of silver nanowires using the TPS technique [36].

30 nm, 50 μm and 60 m^2/g, respectively) were mixed with potassium hydroxide in 1:20 mass proportions. The mixture was then ball-milled for 12 h followed by repeated dilution with distilled water, filtration and washing until no alkalescence was observed. FTIR spectra for the pristine and treated CNT differed greatly, thus indicating surface modification effects. The treated CNT (TCNT) were dried for 24 h at 100 °C and then were dispersed in melting 98% palmitic acid (PA) (density of 853 kg/m^3, MT of 62.4 °C and latent heat of 208 J/g, Sinopharm Chemical Reagent Co., Ltd, Shenzhen, China) without any surfactant and then subjected to intensive sonication. Mixtures with mass fractions of 0.2, 0.5 and 1% were subjected to SEM and their thermal conductivity was determined using the transient short-hot-wire technique (uncertainty less than 1%) that utilized a platinum wire (diameter of 70 μm). A careful procedure for collecting thermal conductivity data in the liquid phase was outlined, however, the details of measurement procedures below the melting temperature were not discussed. Average values of three measurements at each temperature were reported for both solid and liquid phases in 10 and 5 °C intervals, respectively. The latent heat and melting temperature were measured using DSC in the temperature range of 15–70 °C subject to a heating rate of 5 °C/min. Measured values of the thermal conductivity of the mixtures for both liquid and solid phases are plotted against the temperature of the samples in Fig. 31. For a given temperature, the thermal conductivity of both liquids and solids is observed to rise monotonically upon addition of the MWNT. The thermal conductivity is observed to depend weakly on the temperature for temperatures lower than 55 °C and higher than 65 °C, on both sides of the MT of 62.4 °C. Near the melting temperature of the composites, an abrupt rise of thermal conductivity of the solid phase is observed due to enhancement of molecular vibrations in the orderly solid structure. Upon melting, the thermal conductivity declines due to transformation of an orderly structure into the random molecular structure of the liquid state. The thermal conductivity of the solid phase is consistently higher than the value measured for the same sample in its liquid state. The thermal conductivity enhancement index for both phases depended strongly on the mass fraction but exhibited mild variation with temperature. The authors compared the thermal conductivity enhancement index of their treated MWNT to those reported earlier by them [26] with a treatment based on chemical oxidation with a concentrated acid mixture. The composites prepared by the latter treatment exhibited a marked improvement (e.g. factors of 3.5 and 5 for the 1 mass fraction samples at 25 and 70 °C, respectively). Finally, lowering of the melting temperature and latent heat as functions of mass fraction of the CNT, that are in concert with observations of other investigators was reported.

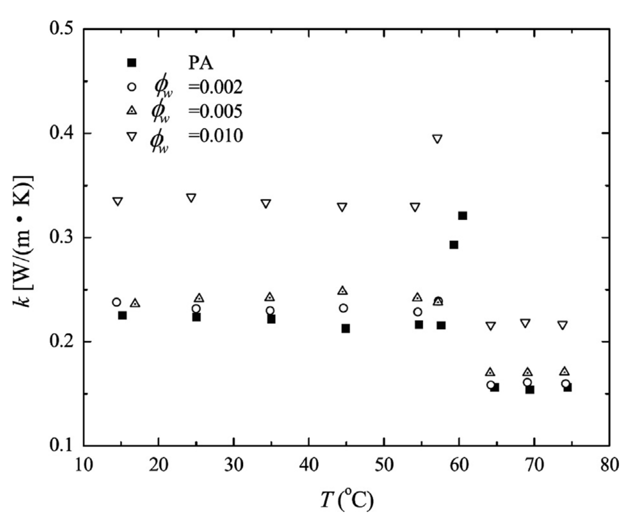


Fig. 31. Temperature-dependent thermal conductivity of palmitic-acid-based phase change materials with multi-walled carbon nanotubes using the THW method [37].

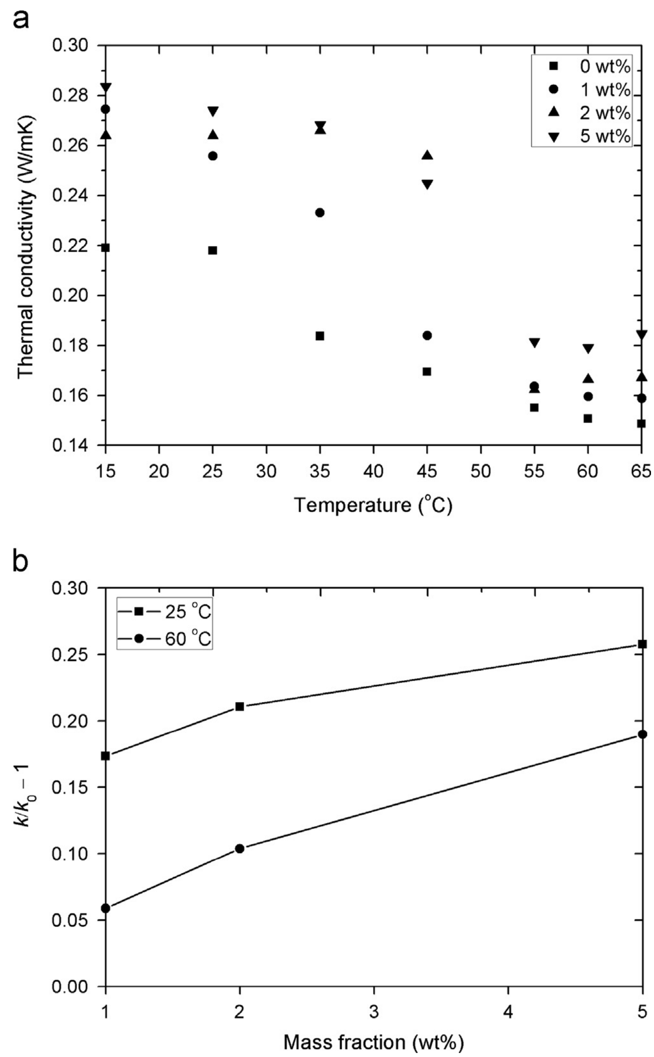


Fig. 32. Variations of (a) temperature-dependent thermal conductivity for both phases and (b) the relative percentages of conductivity enhancement of paraffin-wax-based phase change materials with alumina nanoparticles using the THW technique [38].

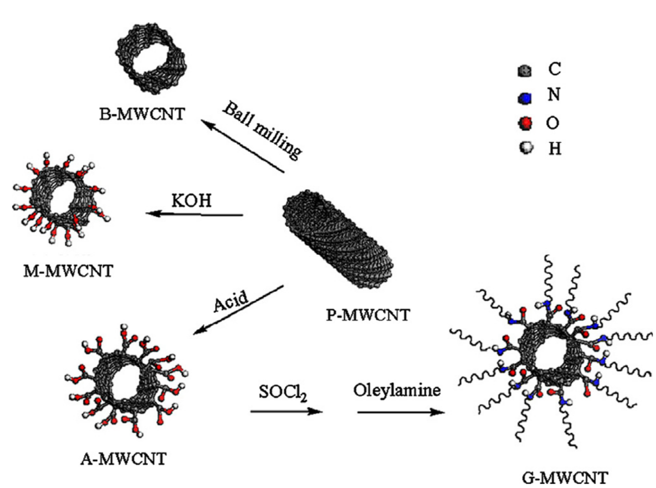


Fig. 33. Schematic diagram of the chemical and mechanical treatment routes of multi-walled carbon nanotubes [39].

Wang et al. [38] added 99.9% purity Al_2O_3 nanoparticles (Hangzhou Jingtian Nanotech. Co., Ltd.) to melting industrial grade paraffin wax (MT of 325–327 K and latent heat of 142.2 J/g, Sinopharm Chemical Reagent Co., Ltd, Shenzhen, China), within which oleylamine was already dispersed as surfactant. The average diameter and density of the nanoparticles were 20 nm (verified via SEM and TEM) and 3.9 g/cm^3, respectively. FTIR tests were performed on the nanoparticles and XRD data confirmed that the structure was γ-phase. The mixture was subjected to intensive sonication. The nanoparticle component of the colloidal systems was identified to be 1, 2 and 5 wt%, even though the exact percentage of the surfactant was not disclosed. Thermal conductivity of the colloidal system was determined using the transient short-hot-wire technique (uncertainty less than 1%) that utilized a platinum wire (diameter of 70 μm), whereas the latent heat (both solid–solid and solid–liquid), melting temperature and solid–solid phase change temperature were measured using DSC in the temperature range of 273–348 K subject to a heating rate of 5 °C/min. The measured latent heat of the PW/Al_2O_3 mixtures was consistently lower than the value for the paraffin wax without additives. The measured melting temperature was also lower than that of the paraffin wax without nanoparticles, except for the 1 wt % sample. The measured thermal conductivity of the mixtures is presented in Fig. 32a. Generally, as the temperature of the sample is raised, its thermal conductivity in the solid phase decreased. At a given temperature, the thermal conductivity of the samples was consistently greater than the base PCM exhibiting a monotonic trend as the particle loading was raised, however, the monotonic behavior was not observed at 288 and 318 K. In the liquid phase, the measured thermal conductivity of the colloidal systems was observed to rise monotonically with increasing mass fraction. The thermal conductivity enhancement ratio exhibiting rising trends with the mass fraction at two temperatures – one solid and one liquid – are plotted in Fig. 32b.

With the intention of elucidating the effect of pre-treatment of the CNT on the interfacial thermal resistance and thermal conductivity of CNT/PCM composites, Wang et al. [39] reported on four methods of treating pristine MWCNT (Chengdu Organic Chemicals Co., Ltd., Chinese Academy of Sciences with average diameter, average length and specific surface area of the CNTs being 30 nm, 50 μm and 60 m^2/g, respectively). Identifying each treated CNT by an appropriate prefix, the schematic diagram of Fig. 33 provides visual representations for the routes of acid oxidation (A-) [26], mechano-chemical reaction (M-) [37], ball milling (B-) [35] and grafting following acid oxidation (G-). As for the last preparation scheme, A-MWCNT were boiled in $SOCl_2$ (containing dimethylformamide) at 70 °C for 48 h. Upon subjecting the mixture to centrifuging, the remaining solid was washed with anhydrous tetrahydrofuran and dried under vacuum. Introduction of 9-octadecen-1-amine group onto the surface of the CNT involved further stirring of the mixture at 70 °C for 120 h. Upon washing with ethanol to remove excess 9-octadecen-1-amine, the black solid was dried under vacuum at room temperature. Regardless of the pre-treatment route, CNT were added into molten 98%-pure PA (MT of 62.5–64 °C, Sinopharm Chemical Reagent Co., Ltd, Shenzhen, China) and subjected to intensive sonication. Various analytical methods including TEM, SEM, FTIR and XRD were utilized for characterization, whereas the transient short-hot-wire technique (uncertainty less than 1%) that utilized a platinum wire (diameter of 70 μm) was used for determination of thermal conductivity. Comparing TEM micrographs of treated MWCNT, the pristine samples were both aggregated and entangled, thus exhibiting poor stability upon forming a suspension. The chemical and/or mechanical treatments helped to break the MWCNT thus helping with their stability. FTIR spectra of the treated MWCNT also showed detectable transmission bands in comparison to the pristine samples. Thermal conductivities of various PA/MWCNT (mass fractions of 0.002, 0.005 and 0.01) were measured at 25 and 70 °C as representatives of the solid and liquid states, respectively. The thermal conductivity enhancement ratios are presented in Fig. 34a and b for the solid and liquid phases, respectively. For a specific composite tested at a given temperature, the thermal conductivity was consistently raised as the mass fraction was increased. For both liquid and solid samples considered with the highest loading of 1 wt%, the M-MWCNT/PA composite exhibited the highest thermal conductivity enhancement ratio in comparison to other composites, i.e. 51.6 and 42.3%, respectively. For the liquid samples, P-MWCNT/PA had the lowest thermal conductivity. The variations of thermal conductivity of various 1 wt% mixtures as a function of temperature are given in Fig. 35. Excluding G-MWCNT/PA composites, the thermal conductivities of the treated samples showed little sensitivity to temperature variation when the measurements were conducted above 63 and below 55 °C. The sudden rise of thermal conductivity of solid samples as the melting temperature is reached followed by its sudden decline was already discussed by Wang et al. [26,35,37]. Tabulation of thermal conductivity enhancement ratios for 1 wt% loading for all tested temperatures revealed that M-MWCNT/PA composites exhibited the highest enhancement, whereas the enhancement of all samples in solid state was higher than those in the liquid state (except G-MWCNT/PA).

Mixtures of paraffin (99.99% purity with MT of 58–60 °C, Shanghai Specimen and Model Factory, China) and copper nanoparticles (Shenzhen Junye Nano Material Ltd., China, with average diameter, purity and specific surface area being 25 nm, 99.9% and

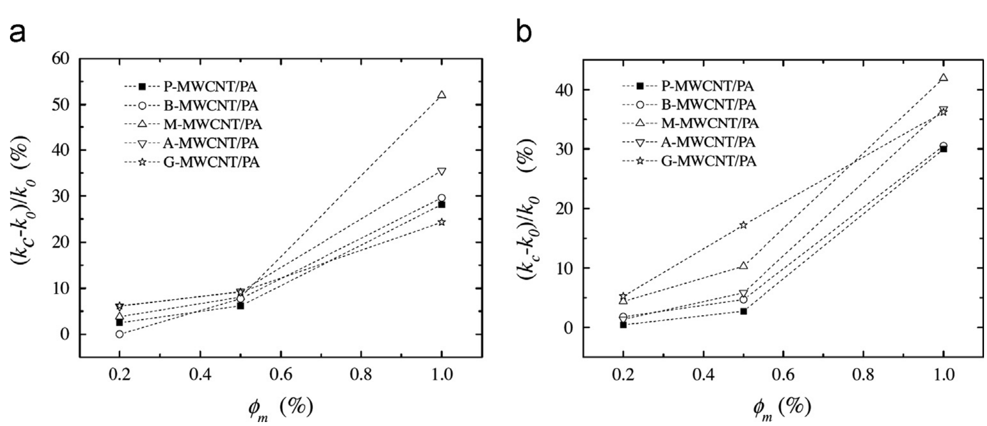


Fig. 34. Relative thermal conductivity enhancement of palmitic-acid-based mixtures with various types of treated multi-walled carbon nanotubes in both (a) solid and (b) liquid phases, using the THW method [39].

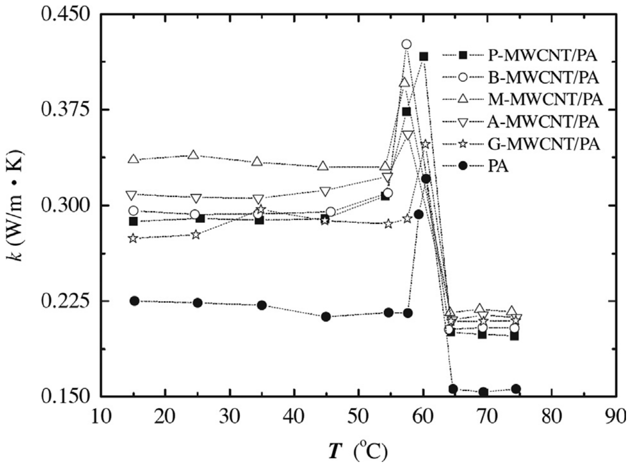


Fig. 35. Temperature-dependent thermal conductivity of 1 wt% palmitic-acid-based mixtures with various types of treated multi-walled carbon nanotubes using the THW technique [39].

30–50 m^2/g, respectively) were prepared by Wang et al. [40]. Gum Arabic in chemical grade (Shanghai Lingfeng Reagent Co. Ltd., China) that is an anionic surfactant was used to coat the nanoparticles (mass ratio of 0.5). The treated nanoparticles were then dispersed in melting paraffin and the suspensions (0.1, 0.5, 1 and 2 wt%) were stirred thoroughly and ultrasonicated for at least 1 h, while maintained above the melting temperature. DSC testing in the 20–80 °C range at a rate of 5 °C/min was carried out. The melting temperatures of the composites differed from that of pure paraffin by less than 0.5 °C, whereas the latent heat of fusion was consistently lowered as the particle loading was increased. Heating and cooling of 50 g samples placed in glass tubes were performed within 70 and 25 °C water baths, respectively, while the temperature at the center of the samples was recorded. The observed faster melting and freezing time durations were attributed to enhancement of thermal conductivity of paraffin–Cu composites.

Starting with three types of nanoparticles (Al, C/Cu and Cu with an average particle size of 25 nm supplied by Shenzhen Junye Nano Material Ltd., China), Wu et al. [41] prepared 0.1 wt% composites with paraffin (58–60 °C, Shanghai Specimen and Model Factory, China) and subjected these to cooling/heating tests (30 and 70 °C water baths). Since the copper-based colloidal systems exhibited faster heating/cooling, combinations with five surfactants (GA, Span-80, CTAB, SDBS, all supplied by Guangzhou Chemical Reagent Factory, China, and Hitenol BC-10, Montello, Inc., Japan) were studied in greater detail. Keeping the copper to dispersant mass ratio at 1:3, Hitenol BC-10 was determined to be the most stable mixture after a 12 h observation period. DSC testing (−10 to 80 °C at a rate of 10 °C/min in N_2 environment) of mixtures with 0.1, 0.5, 1, and 2 wt% revealed little sensitivity of the freezing and melting temperatures, whereas the measured values of heat of fusion were found to be lower than values predicted by the theory of mixtures. The observed faster heating/cooling rates were related to very limited enhanced thermal conductivity data that were obtained using the transient hot wire method. A 0.5 wt% Cu–paraffin composite was also subjected to DSC testing after 20, 50, 70 and 100 thermal cycling tests. The observed deviations in melting/freezing temperatures and latent heat were less than 1.9 and 3.2%, respectively.

In order to explore the effect of carbon nanotubes and surfactant on solidification of deionized water, Mo et al. [42] used 3 types of multi-walled nanotubes (MWNT) with average length of 5–15 μm and average SEM-verified diameters in three ranges of 10–30, 40–60 and 60–100 nm (used as identifiers, i.e. 1030, 4060 and 60,100), supplied from Shenzhen Nanotech Port Co., Ltd (Shenzhen, China). Upon adjusting the pH value of deionized water to 8 using ammonia, nanotubes were added. Sodium dodecyl sulfate ($C_{12}H_{25}SO_4Na$) supplied by Guangdong Xilong Chemical Materials Co., Ltd., China, was used as the surfactant. With a 0.1% mass percentage of the 10–30 nm diameter MWNT additives, samples of three surfactant mass percentages of 0.05, 0.1 and 0.16% were prepared. Moreover, samples of three lengths of MWNT with 0.1% mass percentage of both nanotubes and surfactants were prepared. The samples were stirred using a magnetic stirring apparatus for 20 min followed by ultrasonication (frequency of 20 kHz and power of 100 W) for 60 min at 25–30 °C. Thermal response of the samples was monitored while placed into test tubes and immersed into a −13 °C constant-temperature bath. The effect of the mass concentration of the surfactant on the phase change behavior of the samples is shown in Fig. 36. Upon adding the nanotubes and promoting heterogeneous nucleation, the supercooling temperature was consistently but non-monotonically raised in comparison to deionized water with the 0.1% mass of surfactant sample exhibiting the lowest supercooling temperature. The degrees of supercooling were 1.5, 2.1 and 0.2 °C corresponding to surfactant mass percentages of 0.05, 0.1 and 0.16%, whereas this number was 6.7 °C for deionized water. The phase change temperature was found to be almost insensitive to the mass concentration of the nanotubes and surfactant. Similar tests were performed to assess the effect of the diameter of the nanotubes while keeping the mass concentration of the surfactant and nanotubes constant, i.e. 0.1 wt% in Fig. 37. The samples with the smallest diameter of the nanotubes showed marked easement of supercooling whereas the higher diameter samples performed similar or inferior to deionized water.

Composites of carbon nanofibers and carbon nanotubes with soy wax and paraffin wax were prepared by Cui et al. [43]. Soy wax (a hydrogenated form of soybean oil and natural wax) and paraffin wax with melting temperature of 52–54 °C and room temperature thermal conductivity of about 0.32 W/mK were obtained from Candlewic (Doylestown, PA). Heat-treated carbon nanofibers (Pyrograf Products, Inc., Cedarville, OH) with average diameter of 200 nm and 95% pure multi-walled carbon nanotubes supplied by Chengdu Organic Chemicals Co., Ltd., Chinese Academy of Sciences (www.timesnano.com) with average diameter, average length and specific surface area of 30 nm, 50 μm and 60 m^2/g, respectively, were used. The nanofibers and nanotubes were mixed with molten PCM at 60 °C followed by high-speed stirring for 30 min

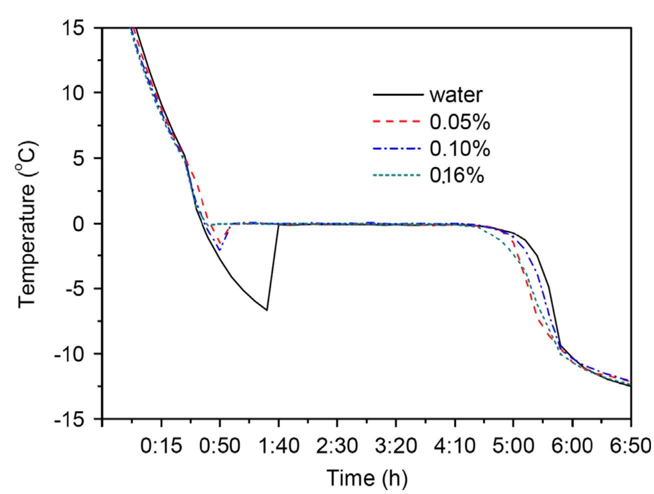


Fig. 36. Comparison of the freezing curves of DI water-based nanofluids with 10–30 nm diameter multi-walled carbon nanotubes as a function of mass fraction of the surfactant [42].

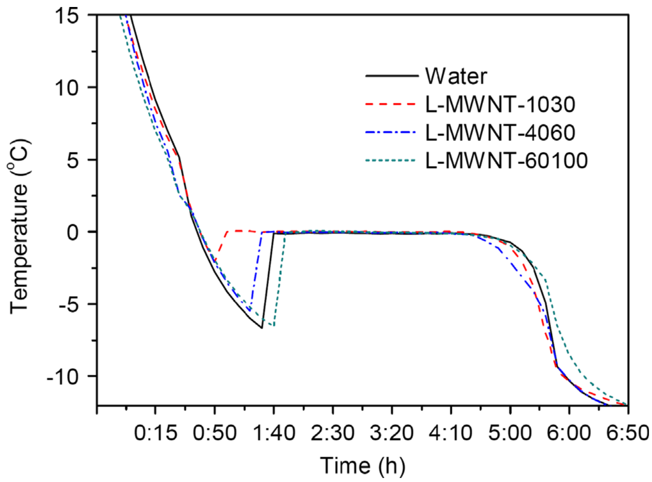


Fig. 37. Comparison of the freezing curves of DI water-based nanofluids with various diameters of multi-walled carbon nanotubes with a surfactant concentration of 0.1% by mass [42].

and ultrasonication for 1 h at the same temperature. A cylindrical module with a cold top surface (50/50 water and ice mixture) and hot bottom surface (Kapton resistance heater) as its horizontal ends were used for melting experiments. The molten samples were poured gently into the module that was also instrumented with type K thermocouples and allowed to solidify. Samples of 1, 2, 5 and 10 wt% were subjected to SEM and DSC (0–75 °C at a rate of 5 °C/min in N_2 environment), whereas their thermal conductivity at room temperature was obtained using the transient hot wire technique (KD2 PRO, Decagon Devices, Pullman, WA). Measured thermal conductivity of soy wax/CNF and soy wax/CNT samples exhibited enhancement as the mass percentage of the additives was raised with the CNF-based samples consistently showing greater enhancement. The greater enhancement of thermal conductivity with CNF translated into faster temperature rise of the samples once the samples were heated, however, reported testing was limited to the solid phase measurements.

Xiang and Drzal [44] studied composites of paraffin wax and exfoliated graphite nanoplatelets (xGnP) of two sizes and aspect ratios in relation to enhancement of electric conductivity, thermal conductivity and latent heat storage. Starting with a stock of sulfuric acid-intercalated expandable graphite (Asbury Graphite Mills, Inc., Asbury, NJ) and thermal treatment, xGnP-15 nanoplatelets (average diameter of 15 μm, thickness of about 10 nm and surface area of 20–40 m^2/g) resulted after sonication for 2 h (same materials discussed above by Kim and Drzal [27]). The xGnP-15 nanoplatelets were then subjected to ball milling for 72 h to reduce the average diameter to 1 μm (thus termed sample xGnP-1) and increase the surface area to 100–130 m^2/g. The paraffin wax (*n*-docosane as described earlier by Kim and Drzal [27]) was melted at 80 °C and nanoplatelets were added under constant stirring to form 1, 2, 4, 6, 8 and 10 wt% composites of paraffin/xGnP. For loading above 6 wt%, xylenes were added to dissolve paraffin first. Liquid samples were dip-sonicated for 1 h prior to evaporation of the solvent. Five millimeter thick and 1 in. diameter specimen were molded for subsequent experiments. Some samples were further processed to a 0.4–0.5 mm thick sheet by a two roll mill for 10 min in order to study the effect of particle orientation on thermal conductivity (in-plane and through-plane measurements at 20 °C under an applied load of 20 psi using the ASTM E1530 standard). DSC-based measurements were performed at a rate of 5 °C/min. Measured through-plane thermal conductivity of paraffin/xGnP molded composites at 20 °C is shown in Fig. 38a with the xGnP-15 nanocomposites exhibiting a linear dependence on volume fraction for low particle loading followed

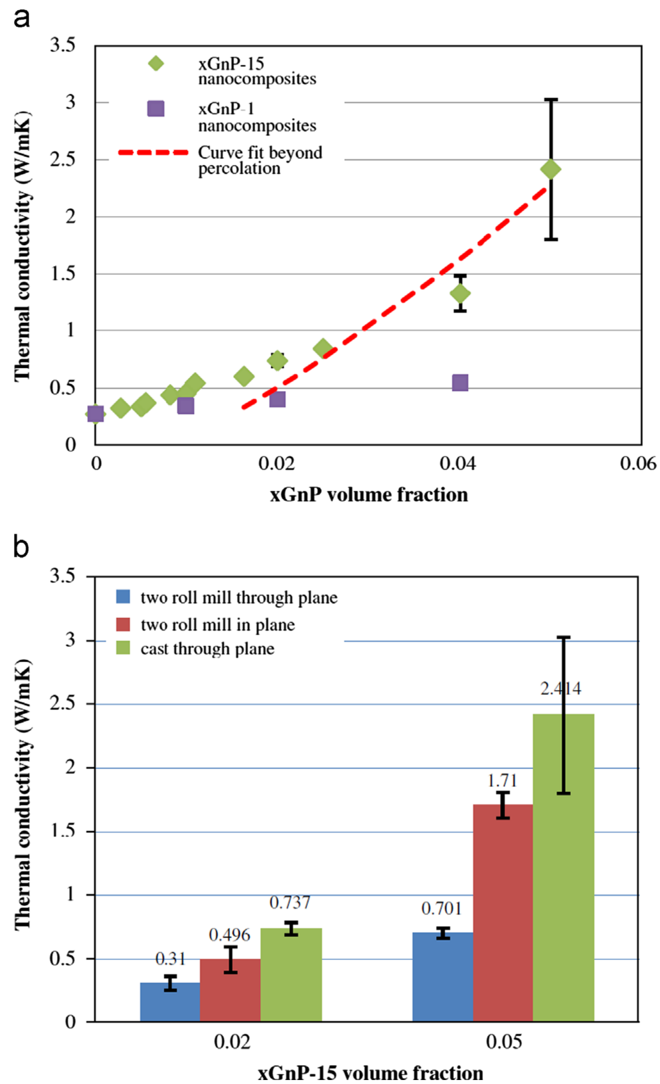


Fig. 38. Measured thermal conductivity of the paraffin/xGnP composites for (a) untreated and ball milling-processed xGnP and (b) untreated and two roll mill-processed xGnP in two directions, using the steady-state method [44].

by a greater level of enhancement at higher particle loadings. The prediction of the nanotube-relevant model of Foygel et al. [45] is also shown by the dashed line. The thermal conductivity enhancement of the xGnP-1 nanocomposites is not as pronounced as the xGn-15 samples due to the greater phonon scattering thermal interface resistance of the smaller particles. Given the superiority of the xGnP-15-based composites, two samples of 2 and 5 vol% paraffin/xGnP-15 composites were prepared by the two roll mill process. Measurements of through-plane and in-plane thermal conductivities for these samples are presented in Fig. 38b with the in-plane thermal conductivities being greater that the through-plane values for both roll mill samples and the molded composites exhibiting the greatest enhancement. Competitions among phonon scattering in relation to random vs. aligned orientations were further elaborated by the authors who also predicted the thermal interface resistance using the model of Nan et al. [46] for nanotubes composites. Based on DSC test results, temperatures that characterize the solid–solid transformation and melting/crystallization peaks were not affected markedly by the presence of xGnP. Similar observations were made for the latent heat values.

Yavari et al. [47] dispersed graphene sheets (estimated theoretical thermal conductivity of 4840–5300 W/mK) in a 25 mL/mg acetone solution that was ultrasonicated for 1.5 min. The mixture

was then heated on a hot plate to 120 °C while being sonicated for another 5 min. 1-Octadecanol (stearyl alcohol with a melting temperature of ~66 °C, heat of fusion of ~250 kJ/kg, thermal conductivity of 0.38 W/mK and density of 0.812 g/cm^3) was then mixed with the graphene solution and was sonicated for another 15 min on a hot plate maintained at about 120 °C. The mixture was then stirred and heated to about ~150 °C in order for the acetone to evaporate. Suspensions containing a maximum of 4 wt% graphene were poured into preheated cylindrical silicone rubber molds (~6.35 mm thick and ~12.7 mm in diameter) and were left to solidify at room temperature for about 20 min. The solid composites were then cut to different thicknesses and polished on a sand paper pad. Uniformly dispersed graphene flakes were observed in the TEM images. A steady-state one-dimensional heat conduction method was utilized for measurement of the thermal conductivity of the solid sample and the corresponding results are shown in Fig. 39. The thermal conductivity of the composites increased in response to greater mass fraction of the graphene flakes with the 4 wt% sample exhibiting a thermal conductivity that is 2.5 times greater than pure 1-octadecanol. It was suggested that the path of lower resistance to phonon transport accommodated by the network of graphene additives, in addition to graphene's high aspect-ratio, large interface contact area and strong interface between the PCM and graphene were the contributors to the observed enhancement. The phase change enthalpy of the 4 wt% sample was lowered by 15% whereas the melting temperature did not vary significantly with the loading of graphene.

Cyclohexane-based NePCM samples were prepared using copper oxide (CuO) nanoparticles with various loadings (0, 1, 2 and 4 wt%) by Fan and Khodadadi [48]. Cyclohexane (C_6H_{12}) (MT of 6.5 °C and heat of fusion of 32,557 J/kg obtained from Pharmco-Aaper, Brookfield, CT, 99.96% purity) is a cycloalkane used as a non-polar solvent in the chemical industry. Due to its transparency in both phases, it has been preferred and widely used in visualized freezing experiments. The CuO nanoparticles, stabilized by sodium oleate acid (SOA) and possessing an average diameter of 9 nm, were synthesized and supplied by colleagues in the Department of Chemistry and Biochemistry [49]. In-house-prepared CuO nanoparticles were available as the first step of a chemical protocol for attaining higher thermal conductivity copper nanoparticles. Despite low value of thermal conductivity of bulk CuO that is far below that of pure copper or other high-conductivity nanostructures, these oxide nanoparticles were utilized. A two-step mixing procedure was followed to prepare the colloidal suspensions however due to pre-treated nature of the nanoparticles with SOA surfactant, this study is distinctly different than all other papers reviewed above where surfactants were added to PCM and nanostructures. Moreover, sonication of the mixtures was deemed unnecessary due to pre-treatment of the nanoparticles with SOA. A HotDisk Thermal Constants Analyser (HotDisk AB, Gothenburg, Sweden) was used to measure the thermal conductivity of the cyclohexane-based NePCM samples. With the aid of a constant-temperature bath (TC-502P, Brookfield Engineering, Middleboro, MA), measurements were performed consecutively at multiple temperatures for samples in both liquid and solid phases and the details of the procedures are given by Fan and Khodadadi [48]. The measured thermal conductivities of the cyclohexane/CuO colloidal systems are presented in Fig. 40a and b. It is observed that thermal conductivity of the samples in their liquid phase is inversely related to temperature. The data for pure liquid cyclohexane measured by Watanabe and Kato [50] are in excellent agreement with the present data, thus verifying the accuracy of the adopted measurement technique. At each of the measured temperatures, monotonic enhancement of thermal conductivity with increased loading of nanoparticles is clearly observed. At 30 °C, the relative enhancement becomes more marked, probably due to more intensive diffusion of nanoparticles, e.g. Brownian and thermophoretic diffusion, at higher temperatures. For samples in the solid phase, the thermal conductivity is

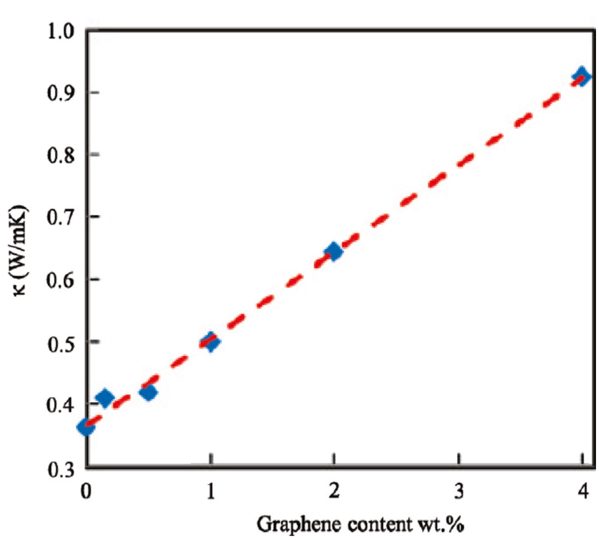


Fig. 39. Measured thermal conductivity of the 1-octadecanol/graphene composites as a function of mass fraction of the graphene additives using the steady-state technique [47].

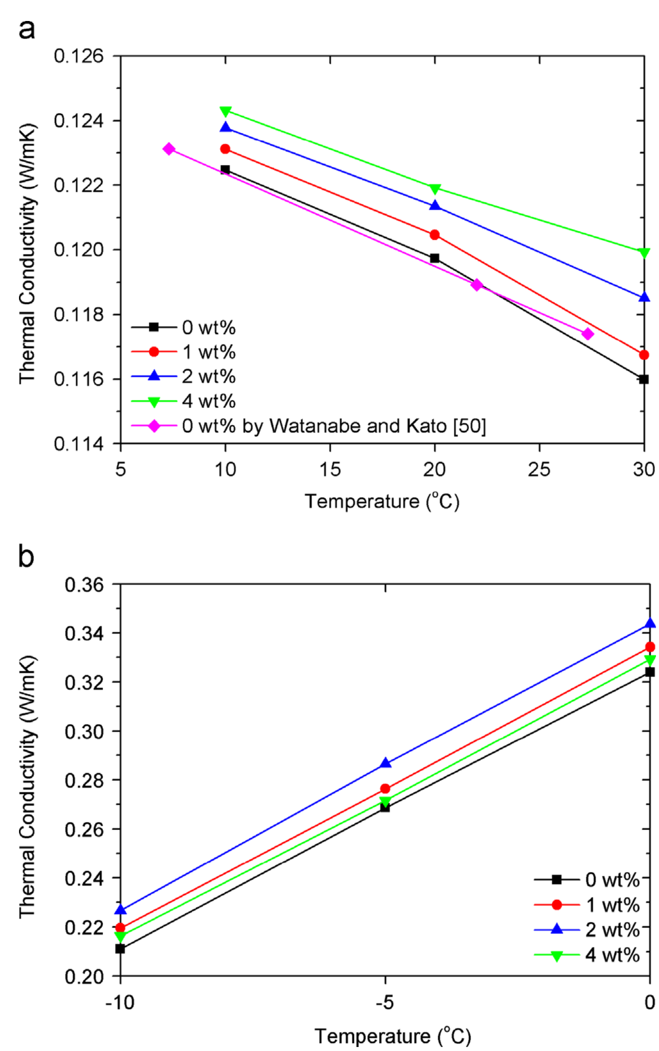


Fig. 40. Measured thermal conductivity of the cyclohexane-based NePCM samples in both (a) liquid and (b) solid phases as a function of mass fraction of the CuO nanoparticles using the TPS technique [48].

found to strongly depend on and almost linearly proportional to temperature (Fig. 40b). It is also observed that at each of the measured temperatures, the enhancement of thermal conductivity is not generally monotonic with the mass fraction of nanoparticles. The exception is observed for the most concentrated sample (4 wt%) investigated. The values for the 4 wt% sample are even less than those for 1 and 2 wt% samples and are only slightly greater than that for pure cyclohexane. It seems that some other phenomenon overshadows the expected monotonic enhancement of thermal conductivity for the solid phase. In the absence of visible precipitation and lack of optical size measurements or transmission electron microscopy information to substantiate clustering of nanoparticles in the solid phase or its nonexistence, the lowering of thermal conductivity upon increasing the weight percentage from 2 to 4 remains unresolved at this time. Unidirectional freezing of the cyclohexane-based NePCM samples was also investigated [48] within an insulated transparent cell that accommodated freezing of the sample from bottom in order to minimize thermal instability issues. Thermocouple readings were recorded at uniform spacings along the freezing direction to allow indirect determination of the process of freezing. Expedited freezing of the colloidal cyclohexane-based system was realized by introducing CuO nanoparticles and the results were compared to a theoretical model.

Using the same approach of Fan and Khodadadi [48], thermal conductivity of eicosane-based NePCM samples was measured by Fan and Khodadadi [51]. Eicosane ($C_{20}H_{42}$) (obtained from Sigma-Aldrich, St. Louis, MO, 99% pure) that is an alkane with a melting point of about 37 °C is a white wax-like solid at room temperature. The samples were prepared with the same SOA-stabilized CuO nanoparticles [49] with mass fractions of 0, 1, 2, 5 and 10 wt%. The measured thermal conductivity data in the liquid phase exhibit an inverse relation to temperature (Fig. 41). At 60 °C, the measured value for pure eicosane (0.1432 W/mK) agrees fairly well with that available in the literature, i.e., $k=0.1442$ W/mK [34]. In that reference, thermal conductivity data for liquid eicosane at atmospheric pressure above 60 °C are also available and an almost linear-decay correlation with temperature is shown up to 200 °C. For the temperature range close to the melting point of eicosane (~37 °C), the thermal conductivity becomes less sensitive to temperature variation. It was observed that as the mass fraction of nanoparticles was increased, more marked enhancement of thermal conductivity was obtained. At constant particle loadings, the enhancement generally becomes greater at higher temperatures. The greatest enhancement is found to be nearly 7% for the 10 wt% sample at 60 °C. It was also found that the measured data agree well with the predicted values of Maxwell's equation (Eq. 2). Great uncertainties associated with the measured data of eicosane-based NePCM samples in the solid phase clearly indicated the influence of the formation schemes on the measurements, especially for solid samples with a base PCM having significant supercooling upon solidification. Possible reasons were discussed in regard to the requirement of sample preparation of the transient plane source (TPS) technique.

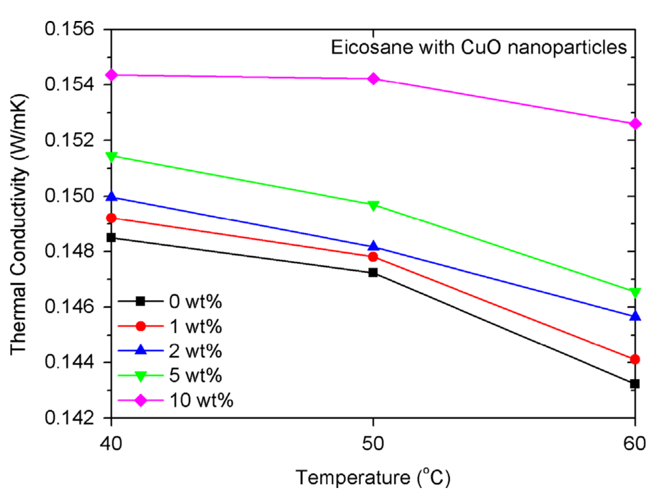


Fig. 41. Measured thermal conductivity of eicosane-based NePCM samples in the liquid phase as a function of mass fraction of the CuO nanoparticles using the TPS method [51].

5. Summary of reviewed work

Having reviewed all the known publications of nanostructure-based colloidal suspensions that were intended for thermal energy storage, categorization of these studies based on type of materials, preparation routes, adopted techniques, etc. is possible.

5.1. Classification of the adopted nanostructure-enhanced PCM

The 4 categories of the utilized nanostructures, namely *carbon-based nanostructures, carbon nanotubes, nanoparticles* and *nanowires* are summarized in Table 3. For carbon-based nanostructures, more exact subgroupings are identified. One can note that corresponding to the relevant entries of Tables 1 and 2, the entries of Table 3 were filled chronologically. Moreover, the suppliers of the specific materials and dimensions of the nanostructures (if available) are provided in Table 3, whereas some researchers including the present authors utilized nanostructures that were developed in-house. Carbon-based nanostructures (category A) included nanofibers, nanoplatelets and graphene flakes [17,23,25,27,43,44,47]. Interestingly, as for the carbon nanotubes (category B), MWCNT with diameters in the 10–100 nm range were supplied by only two companies and were utilized by 8 studies [24,26,28,35,37,39,42,43]. Considering nanoparticles, both metallic (Ag [21], Al [41], C/Cu [41] and Cu [40,41]) and oxide (Al_2O_3 [20,22,30–32,38], CuO [48,51], MgO [20] and TiO_2 [22,29]) materials with diameters in the range 5–500 nm were employed. Only one study used silver nanowires [36].

5.2. Preparation routes for developing nanostructure-enhanced PCM

All the 20 studies that were reviewed above except Zeng et al. [21] employed the *two-step* method whereby the two main constituents, namely the nanostructures of interest and the liquid PCM, were mixed. Generally, surfactants that are listed in Table 2 (Anhydrous Ethanol [36], CTAB [28,41], Gum Arabic [40,41], Hitenol BC-10 [41], Oleylamine [38], SDBS [19,20,28,30,41], SDS [42], SINO-POL20 [31,32] and SPAN-80 [41]) were added to promote the stability of dispersions and the resulting mixtures were then sonicated/ultrasonicated in order to break down agglomerated nanostructures and promote stability. Exceptions to this general approach exist as exercised by some researchers. Elgafy and Lafdi [17] and Zeng et al. [21] did not use surfactant/sonication or did not report such practices. Some researchers only reported using sonication with no mention of surfactants [22–27,35,37,39,43–45], with Liu et al. [29] utilizing a supersonic oscillator. Two of the present authors [48,51] are the only group that utilized nanoparticles pre-treated with surfactant (SOA) and did not use sonication. Despite all these practiced techniques to promote stability of colloidal suspensions, it is well known that such systems tend to precipitate and even exhibit agglomeration during non-phase change experiments, as reported by Gharagozloo et al. [52].

5.3. Adopted thermal conductivity determination techniques

Techniques used for measuring thermal conductivities of matter in different phases are broadly classified into two groups, namely

Table 3
Summary of the nanostructures utilized for thermal conductivity enhancement of phase change materials.

	Supplier	Dimensions, etc.[a]	Authors (year)
A. Carbon-based nanostructures			
Carbon nanofibers (CNF)	Applied Sciences, Cedarville, OH	D=100 nm, L=20 μm	Elgafy and Lafdi (2005) [17]
	Unknown	D=100 nm	Shaikh et al. (2008) [25]
	Pyrograf Products, Inc., Cedarville, OH	D=200 nm	Cui et al. (2011) [43]
Graphite nanofibers	In-house	D=4–10 nm, L=1 μm	Weinstein et al. (2008) [23]
Graphite nanoplatelets	Asbury Graphite Mills, Inc., Asbury, NJ	D=15 μm, t < 10 nm, SSA=30 m^2/g	Kim and Drzal (2009) [27] and Xiang and Drzal (2011) [44]
	Asbury Graphite Mills, Inc., Asbury, NJ	D=1 μm, t < 10 nm, SSA=100–130 m^2/g	Xiang and Drzal (2011) [44]
Graphene flakes	In-house	N/A	Yavari et al. (2011) [47]
B. Carbon nanotubes			
Single-walled nanotubes (SWNT)	Carbon Nanotechnologies Inc., Houston, TX	N/A	Hong et al. (2007) [19,20]
	Unknown	D=1 nm	Shaikh et al. (2008) [25]
Multi-walled nanotubes (MWNT)	Shenzhen Nanotech Port Co., Shenzhen, China	D=10–30 nm, L=5–15 μm	Zeng et al. (2008) [24]
	Unknown	D=10 nm	Shaikh et al. (2008) [25]
	Chengdu Organic Chemicals Co., Ltd., China	D=30 nm, L=50 μm, SSA=60 m^2/g	Wang et al. (2008, 2009, 2010a,b) [26,35,37,39] and Cui et al. (2011) [43]
	Shenzhen Nanotech Port Co., Shenzhen, China	D=10–30 nm, L=5–15 & 1–2 μm	Zeng et al. (2009) [28]
	Shenzhen Nanotech Port Co., Shenzhen, China	D=10–30, 40–60, 60–100 nm, L=5–15 μm	Mo et al. (2011) [42]
C. Nanoparticles			
Alumina (Al_2O_3)	Sigma-Aldrich, St. Louis, MO	N/A	Hong et al. (2007) [20]
Magnesium oxide (MgO)	Sigma-Aldrich, St. Louis, MO	N/A	Hong et al. (2007) [20]
Silver (Ag)	In-house	D=500 nm	Zeng el al. (2007) [21]
Alumina (Al_2O_3)	Unknown	D=8 nm	Xie et al. (2008) [22]
Titanium oxide (TiO_2)	Unknown	D=3.8 nm	Xie et al. (2008) [22]
Titanium oxide (TiO_2)	Unknown	D=20 nm	Liu et al. (2009) [29]
Alumina (Al_2O_3)	Alfa Aesar, Ward Hill, MA	D=20 nm	Wu et al. (2009) [30]
Alumina (Al_2O_3)	Nanotech, Kanto Chemical Co. Inc., Japan	D=33 nm	Ho and Gao (2009) [31] and Gao (2008) [32]
Alumina (Al_2O_3)	Hangzhou Jingtian Nanotech Co., Ltd, China	D=20 nm	Wang et al. (2010) [38]
Copper (Cu)	Shenzhen Junye Nano Material Ltd., China	D=25 nm, SSA=30–50 m^2/g	Wang et al. (2010) [40]
Al	Shenzhen Junye Nano Material Ltd., China	D=25 nm	Wu et al. (2010) [41]
C/Cu	Shenzhen Junye Nano Material Ltd., China	D=25 nm	Wu et al. (2010) [41]
Copper (Cu)	Shenzhen Junye Nano Material Ltd., China	D=25 nm	Wu et al. (2010) [41]
Copper oxide (CuO)	In-house	D=5–15 nm	Fan and Khodadadi (2011) [48,51]
D. Nanowires			
Silver (Ag) nanowires	Shenzhen Nanotech Port Co., Shenzhen, China	D=10–30 nm, L=5–15 μm	Zeng et al. (2006) [36]

[a] In this column, D, L, SSA and t stand for diameter, length, specific surface area and thickness, respectively.

steady-state and transient methods. The steady-state methods that are based on the one-dimensional Fourier's law, including guarded hot plate and heat flow meter techniques, require a long waiting time period to establish a stable thermal gradient within a specimen. Thus, these are well-suited for the solid phase measurements and were adopted by a few researchers reviewed in this paper [23,27,44,47]. The transient techniques, however, provide a rapid means for measuring thermal conductivity within minutes. Transient techniques include transient hot wire (THW), transient plane source (TPS) and laser flash, etc. The transient techniques are particularly suitable for measuring liquid samples as the onset of natural convection would be avoided if a small sample is used and the measurement is completed over a very short time period. Not surprisingly, most of the studies discussed in this paper adopted THW [26,29–32,35,37–39,41,43] and TPS [24,28,36,48,50] techniques for measuring both liquid and solid samples. The laser flash technique was used by Elgafy and Lafdi [17] to measure thermal conductivity indirectly.

5.4. Complete measured raw thermal conductivity data and their reduced form

The complete raw data of measured thermal conductivity of NePCM in both phases as reported in 20 of the reviewed papers (some of which are not shown in previous figures) were extracted by the authors, thus forming a data bank including 343 data points. The relative thermal conductivity that is the ratio of the effective thermal conductivity to that of the pure PCM at the measured temperature as a function of the reported mass fraction (ϕ_{wt}) of the nanofillers enhancers are presented in Fig. 42. Among these 20 papers, 2 studies [29,44] reported values of volume fractions of the nano-enhancers. Thus, appropriate conversion (Eq. (4)) was applied that might entail introduction of uncertainties as discussed below. The pure material data corresponding to relative thermal conductivity of unity are not presented. The specific measurement temperatures cannot be provided in this figure (to be discussed later), thus colored symbols are employed with blue and red denoting solid and liquid phases,

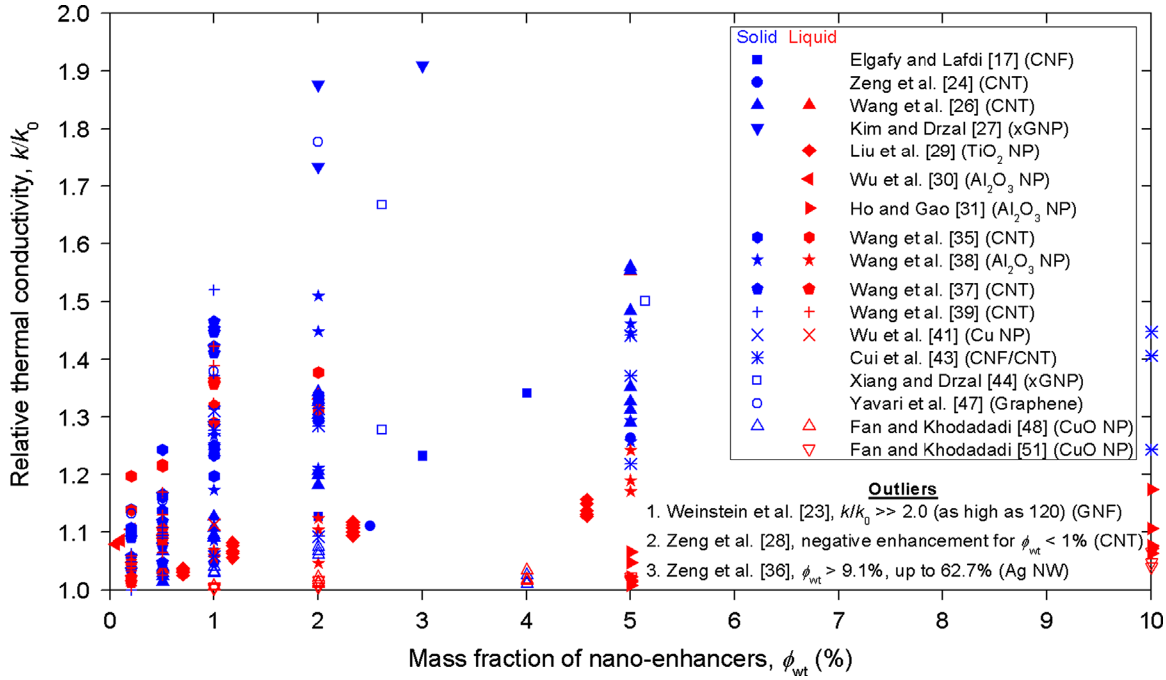


Fig. 42. Collection of measured values of thermal conductivity enhancement of various NePCM samples reported in the reviewed papers as a function of mass fraction of the nano-enhancers, where CNF, CNT, xGNP, NP and NW stand for carbon nanofibers, carbon nanotubes, exfoliated graphite nanoplatelets, nanoparticles and nanowires, respectively.

respectively, and the categories of nano-enhancers are given for each study. Data of 17 studies are presented in Fig. 42. Considering the quality of the presentation of Fig. 42, very few data points from three (3) studies [27,44,47] were excluded since the ranges of presentation for relative thermal conductivity and mass fraction were restricted to 1–2 and 0–10%, respectively. However, measured quantities of 3 papers are not shown. Among these 3 outliers, the relative thermal conductivity data of Weinstein et al. [23] are too high (as high as 120). Zeng et al. [28] reported thermal conductivity data exhibiting lower values than that of the pure materials (negative enhancement) for $\phi_{wt} < 0.01$ (Fig. 16a) and some handful of their enhanced data are not shown. The data of Zeng et al. [36] are not shown since the reported mass fractions were too high (9–63 wt%). Bulk of the reported data shown in Fig. 42 correspond to mass fractions in the 0–0.05 range with the reported relative thermal conductivity for solids generally being greater than the values for the liquid samples. Only 2 research groups, one being the current authors, that represent 6 studies [26,35,37–39,48] have provided detailed temperature-dependent measurements of thermal conductivity in both solid and liquid phases using the THW and TPS techniques. Data of Wu et al. [41] in both phases were reported at unspecified temperatures. Those who reported their data for only a single phase might have done so at a single or multiple temperature(s) and the reader is referred to Table 2 in which an identifier (*SL-xT*) was used to denote such information.

Further discussion of Fig. 42 and extracting more insight from it is not possible. Thus, an attempt was made to come up with a reduced form of the raw data that will allow the reader to gain a deeper understanding of the effect of the temperature and categories of nano-enhancers. The reduction of the raw data was also partially inspired by the asymptotic behavior of the Maxwell's relation (Eq. (2)). For highly conductive additives and small volume fraction, Eq. (2) reduces to

$$M = \frac{\left(\frac{k}{k_0} - 1\right)}{\phi_{vol}} = 3. \tag{6}$$

This reduced form that is called the figure of merit (M) is simply the relative thermal conductivity data of Fig. 42 divided by the volume fraction of the specific sample. This form of presentation allows one to plot M versus temperature, thus allowing grouping of the colloidal systems in both liquid and solid phases. In addition, the reward of greater enhancement due to adding more enhancers is quantified. The values of the figure of merit (M) versus temperature difference (i.e. melting temperature subtracted from the measurement temperature) are shown in Fig. 43. In addition to the obvious uncertainties associated with the temperature difference, there are far more serious concerns with converting the reported mass fractions into volume fractions (Eq. (5)). Due to the unknown nature of the densities of nanostructures, bulk densities of the nano-enhancers were utilized in Eq. (5). For instance, the value of 2100 kg/m^3 was used as the estimated density of all the carbon-based nanostructures. Densities of the base PCM and the reported mass fractions also carry their own uncertainties. In addition to these uncertainties, in order to keep this figure legible and less crowded (unlike Fig. 42), average values of the figures of merit are shown at each temperature.

Two of the outliers [23,28] of Fig. 42 are still considered as outliers in Fig. 43 since data of Zeng et al. [36] are now in the range of presented data. The figure of merit data of Wu et al. [30,41] that were shown in Fig. 42 are too high (>300) and are not shown. Great care was taken to present the colored symbols in concert with the materials categories of Table 3 that is reproduced in the caption. Characters A, B, C and D correspond to carbon-based nanostructures, carbon nanotubes, nanoparticles and nanowires, respectively. Samples containing carbon-based nanostructures and nanotubes consistently exhibit a higher Figure of Merit compared to the nanoparticles. The majority of the data lie above the $M=3$ line. Solid phase measurements (if available) were higher than the liquid phase data. Focusing on the liquid phase, three bars taken from Gharagozloo et al. [52] are adopted. These bars summarize the figure of merit for a great number of nanofluid studies involving oxide nanoparticles, metal nanoparticles and carbon nanotubes.

6. Conclusions

A review of experimental/computational work on an emerging class of PCM modified for enhanced thermal conductivity through

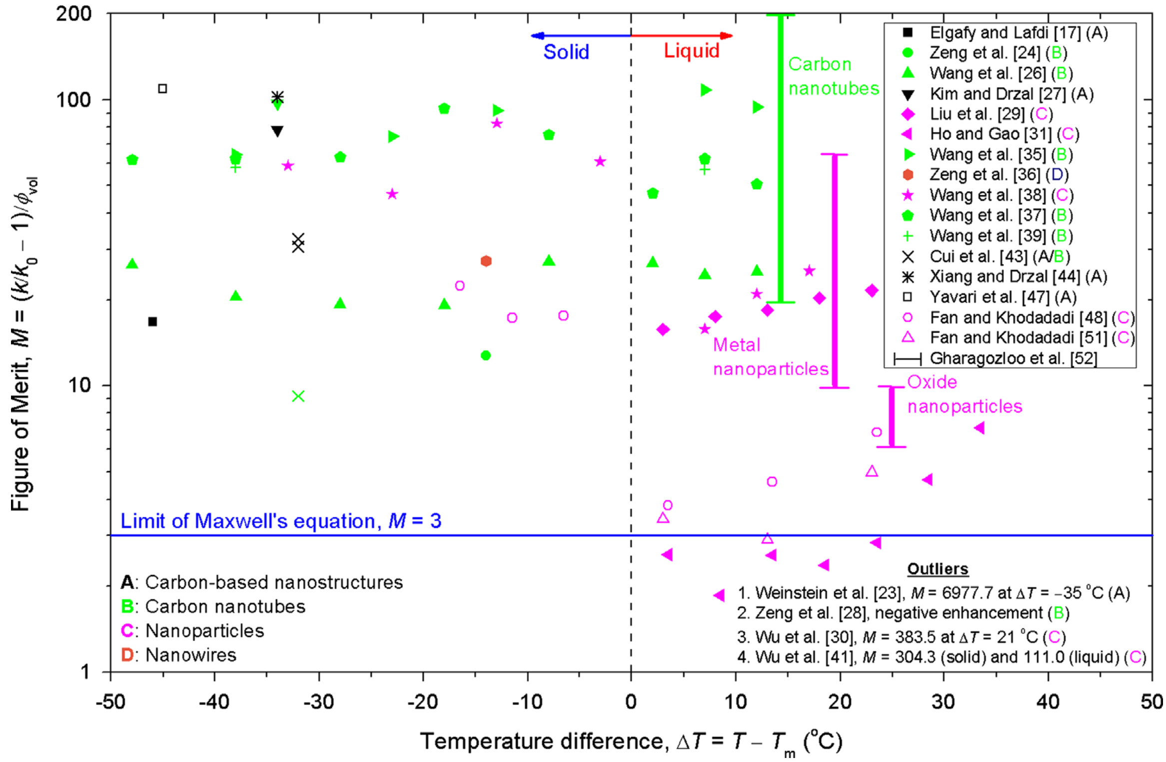


Fig. 43. Figure of merit of the various classes of nano-enhancers as a function of the temperature difference between the temperature of thermal conductivity measurements and melting point of the PCM.

introduction of nanostructures was presented and the following conclusions are made:

1. A clear departure from previous practices of utilizing bulky, fixed, stationary high-conductivity inserts/structures in PCM has been initiated in these recent studies that focus on more versatile nanostructures.
2. A wide range of nanostructures in terms of base materials and geometrical aspect-ratio are utilized as thermal conductivity promoters. These include carbon-based nanostructures (nanofibers, nanoplatelets and graphene flakes), carbon nanotubes, both metallic (Ag, Al, C/Cu and Cu) and metal oxide (Al_2O_3, CuO, MgO and TiO_2) nanoparticles and silver nanowires.
3. In addition to quantifying the improvement of thermal conductivity as functions of temperature and mass fraction of the nanofillers for both solid and liquid phases, effects of adding of nanostructures on the degree of supercooling, melting temperature, viscosity, heat of fusion, etc. are also reported.
4. In general, carbon-based nanostructures and carbon nanotubes exhibit far greater enhancement of thermal conductivity in comparison to metallic/metal oxide nanoparticles. These high aspect-ratio nanoadditivies provide greatly-improved conductive paths when compared to spherical or even agglomoreted nanoparticles.
5. The majority of the 340+ measured thermal conductivity data points in both liquid and solid phases is summarized. Utilizing a figure of merit for the observed thermal conductivity improvements, clear trends for the various nanostructures are exhibited.

Acknowledgment

This material is based upon work supported by the US Department of Energy under Award no. DE-SC0002470 (http://www.eng.auburn.edu/nepcm). The second and third authors, Dr. Liwu Fan and Mr. H. Babaei, also acknowledge financial support provided by the Alabama EPSCoR Program under the Graduate Research Scholars Program (rounds 5 and 6). The third author is grateful to the Samuel Ginn College of Engineering and the Department of Mechanical Engineering at Auburn University for providing support for his Dean's Fellowship since Fall 2009.

This report was prepared as an account of work sponsored by an agency of the United States Government. Neither the United States Government nor any agency thereof, nor any of their employees, makes any warranty, express or implied, or assumes any legal liability or responsibility for the accuracy, completeness, or usefulness of any information, apparatus, product, or process disclosed, or represents that its use would not infringe privately owned rights. References herein to any specific commercial product, process, or service by trade name, trademark, manufacturer, or otherwise do not necessarily constitute or imply its endorsement, recommendation, or favoring by the United States Government or any agency thereof. The views and opinions of authors expressed herein do not necessarily state or reflect those of the United States Government or any agency thereof.

References

[1] Fan L, Khodadadi JM. Thermal conductivity enhancement of phase change materials for thermal energy storage: a review. Renewable Sustainable Energy Reviews 2011;15:24–46.
[2] Das SK, Choi SUS, Yu W, Pradeep R. Nanofluids: science and technology. Wiley-Interscience; 2007.
[3] Batchelor GK. Transport properties of two-phase materials with random structure. Annual Review of Fluid Mechanics 1974;6:227–55.
[4] Progelhof RC, Throne JL, Ruetsch RR. Methods for predicting the thermal conductivity of composite systems: a review. Polymer Engineering & Science 1976;16:615–25.
[5] Maxwell JC. A treatise on electricity and magnetism. Oxford, UK: Clarendon Press; 1873.
[6] Yu W, France DM, Routbort JL, Choi SUS. Review and comparison of nanofluid thermal conductivity and heat transfer enhancements. Heat Transfer Engineering 2008;29:432–60.

[7] Nomura S, Chou T-W. Bounds of effective thermal conductivity of short-fiber composites. Journal of Composite Materials 1980;14:120–9.
[8] Hasselman DPH, Johnson LF. Effective thermal conductivity of composites with interfacial thermal barrier resistance. Journal of Composite Materials 1987;21:508–15.
[9] Nan C-W, Birringer R, Clarke DR, Gleiter H. Effective thermal conductivity of particulate composites with interfacial thermal resistance. Journal of Applied Physics 1997;81:6692–9.
[10] Evans W, Prasher R, Fish J, Meakin P, Phelan P, Keblinski P. Effect of aggregation and interfacial thermal resistance on thermal conductivity of nanocomposites and colloidal nanofluids. International Journal of Heat and Mass Transfer 2008;51:1431–8.
[11] Koo J, Kleinstreuer C. Impact analysis of nanoparticle motion mechanisms on the thermal conductivity of nanofluids. International Journal of Heat and Mass Transfer 2005;32:1111–8.
[12] Koo J, Kleinstreuer C. A new thermal conductivity model for nanofluids. Journal of Nanoparticle Research 2004;6:577–88.
[13] Buongiorno J, et al. A benchmark study on the thermal conductivity of nanofluids. Journal of Applied Physics 2009;106(094312):14.
[14] Hoover MJ, Grodzka PG, O′Neill MJ. Space thermal control development. Lockheed Huntsville Research and Engineering Center Final Report, LMSC-HREC D225500, vol. 81; 1971.
[15] Siegel R. Solidification of low conductivity material containing dispersed high conductivity particles. International Journal of Heat and Mass Transfer 1977;20:1087–9.
[16] Seeniraj RV, Velraj R, Narasimhan NL. Heat transfer enhancement study of a LHTS unit containing dispersed high conductivity particles. Journal of Solar Energy Engineering 2002;124:243–9.
[17] Elgafy A, Lafdi K. Effect of carbon nanofiber additives on thermal behavior of phase change materials. Carbon 2005;43:3067–74.
[18] Khodadadi JM, Hosseinizadeh SF. Nanoparticle-enhanced phase change materials (NEPCM) with great potential for improved thermal energy storage. International Journal of Heat and Mass Transfer 2007;34:534–43.
[19] Hong H, Wensel J, Peterson S, Roy W. Efficiently lowering the freezing point in heat transfer coolants using carbon nanotubes. Journal of Thermophysics and Heat Transfer 2007;21:446–8.
[20] Hong H, Zheng Y, Roy W. Nanomaterials for efficiently lowering the freezing point of anti-freeze coolants. Journal for Nanoscience and Nanotechnology 2007;7:1–5.
[21] Zeng JL, Sun LX, Xu F, Tan ZC, Zhang ZH, Zhang J, et al. Study of a PCM based energy storage system containing Ag nanoparticles. Journal of Thermal Analysis and Calorimetry 2007;87:369–73.
[22] Xie H, Wan J, Chen L. Effects on the phase transformation temperature of nanofluids by the nanoparticles. Journal of Materials Sciences & Technology 2008;25:742–4.
[23] Weinstein RD, Kopec TC, Fleischer AS, D′Addio E, Bessel CA. The experimental exploration of embedding phase change materials with graphite nanofibers for the thermal management of electronics. Journal of Heat Transfer 2008;130 (042405):8.
[24] Zeng JL, Liu YY, Cao ZX, Zhang J, Zhang ZH, Sun XL, et al. Thermal conductivity enhancement of MWNTS on the PANI/tetradecanol form-stable PCM. Journal of Thermal Analysis and Calorimetry 2008;91:443–6.
[25] Shaikh S, Lafdi K, Hallinan K. Carbon nanoadditives to enhance latent energy storage of phase change materials. Journal of Applied Physics 2008;103 (094302):6.
[26] Wang J, Xie H, Xin Z. Thermal properties of heat storage composites containing multiwalled carbon nanotubes. Journal of Applied Physics 2008;104 (113537):5.
[27] Kim S, Drzal LT. High latent heat storage and high thermal conductive phase change materials using exfoliated graphite nanoplatelets. Solar Energy Materials & Solar Cells 2009;93:136–42.
[28] Zeng JL, Cao Z, Yang DW, Xu F, Sun LX, Zhang XF, et al. Effects of MWNTS on phase change enthalpy and thermal conductivity of a solid-liquid organic PCM. Journal of Thermal Analysis and Calorimetry 2009;95:507–12.
[29] Liu Y-D, Zhou Y-G, Tong M-W, Zhou X-S. Experimental study of thermal diffusivity and phase change performance of nanofluids PCMs. Microfluidics and Nanofluidics 2009;7:579–84.
[30] Wu S, Zhu D, Li X, Li H, Lei J. Thermal energy storage behavior of Al_2O_3–H_2O nanofluids. Thermochimica Acta 2009;483:73–7.
[31] Ho CJ, Gao JY. Preparation and thermophysical properties of nanoparticle-in-paraffin emulsion as phase change material. International Communications in Heat and Mass Transfer 2009;36:467–70.
[32] Gao JY. An experimental study on melting heat transfer behavior of a phase-change-material containing Al2O3 nanoparticles in a vertical rectangular enclosure. MS thesis, National Cheng Kung University, Taiwan; 2008. 86 pages (available online at 〈http://ethesys.lib.ncku.edu.tw/ETD-db/ETD-search/view_etd?URN=etd-0825108-153106〉).
[33] Humphries WR, Griggs EI. A design handbook for phase change thermal control and energy storage devices. NASA Technical Paper 1977;1074 (1977):256.
[34] Rastorguev YuL, Bogatov GF, Grigor′ev BA. Thermal conductivity of higher n-alkanes. Chemistry and Technology of Fuels and Oils 1974;10:728–32.
[35] Wang J, Xie H, Xin Z. Thermal properties of paraffin based composites containing multi-walled carbon nanotubes. Thermochimica Acta 2009;488: 39–42.
[36] Zeng JL, Cao Z, Yang DW, Sun LX, Zhang L. Thermal conductivity enhancement of Ag nanowires on an organic phase change material. Journal of Thermal Analysis and Calorimetry 2010;101:385–9.
[37] Wang J, Xie H, Xin Z, Li Y, Chen L. Enhancing thermal conductivity of palmitic acid based phase change materials with carbon nanotubes as fillers. Solar Energy 2010;84:339–44.
[38] Wang J, Xie H, Li Y, Xin Z. PW based phase change nanocomposites containing γ-Al_2O_3,. Journal of Thermal Analysis and Calorimetry 2010;102:709–13.
[39] Wang J, Xie H, Xin Z, Li Y. Increasing the thermal conductivity of palmitic acid by the addition of carbon nanotubes. Carbon 2010;48:3979–86.
[40] Wang N, Yang S, Zhu D, Ju X. Preparation and heat transfer behavior of paraffin based composites containing nano-copper particles. In: Proceedings of the seventh international conference on multiphase flow, Tampa, FL; 2010. 4 pages.
[41] Wu S, Zhu D, Zhang X, Huang J. Preparation and melting/freezing characteristics of Cu/paraffin nanofluid as phase-change material (PCM). Energy and Fuels 2010;24:1894–8.
[42] Mo S, Chen Y, Yang J, Luo X. Experimental study on solidification behavior of carbon nanotube nanofluid. Advanced Materials Research 2011;171-172:333–6.
[43] Cui Y, Liu C, Hu S, Yu X. The experimental exploration of carbon nanofiber and carbon nanotube additives on thermal behavior of phase change materials. Solar Energy Materials and Solar Cells 2011;95:1208–12.
[44] Xiang J, Drzal LT. Investigation of exfoliated graphite nanoplatelets (xGnP) in improving thermal conductivity of paraffin wax-based phase change material. Solar Energy Materials and Solar Cells 2011;95:1811–8.
[45] Foygel M, Morris RD, Anez D, French S, Sobolev VL. Theoretical and computational studies of carbon nanotube composites and suspensions: electrical and thermal conductivity. Physical Review B: Condensed Matter and Materials Physics 2005;71(104201):8.
[46] Nan C-W, Liu G, Lin Y, Li M. Interface effect on thermal conductivity of carbon nanotube composites. Applied Physics Letters 2004;85:3549–51.
[47] Yavari F, Raeisi Fard H, Pashayi K, Rafiee MA, Zamiri A, Yu Z, et al. Enhanced thermal conductivity in a nanostructured phase change composite due to low concentration graphene additives. Journal of Physical Chemistry C 2011;115: 8753–8.
[48] Fan L, Khodadadi JM. An experimental investigation of enhanced thermal conductivity and expedited unidirectional freezing of cyclohexane-based nanoparticle suspensions utilized as nano-enhanced phase change materials (NePCM). International Journal of Thermal Sciences 2012;62:120–6.
[49] Clary D, Mills G. Preparation and thermal properties of CuO particles. Journal of Physical Chemistry C 2011;115:1767–75.
[50] Watanabe H, Kato H. Thermal conductivity and thermal diffusivity of twenty-nine liquids: alkenes, cyclic (alkanes, alkenes, alkadienes, aromatics), and deuterated hydrocarbons. Journal of Chemical & Engineering Data 2004;49: 809–25.
[51] Fan L, Khodadadi JM. Temperature-dependent thermal conductivity of eicosane-based phase change materials with copper oxide nanoparticles. In: International symposium on thermal and materials nanoscience and nanotechnology, Antalya, Turkey; 2011. 8 pages.
[52] Gharagozloo PE, Eaton JK, Goodson KE. Diffusion, aggregation, and the thermal conductivity of nanofluids. Applied Physics Letters 2008;93(103110):3.